

1 **Title:** Single-blind test of nine methane-sensing satellite systems from three continents
2 **Authors:** Evan D. Sherwin^{1,a,*}, Sahar H. El Abbadi¹, Philippine M. Burdeau¹, Zhan Zhang¹,
3 Zhenlin Chen¹, Jeffrey S. Rutherford^{1,b}, Yuanlei Chen¹, Adam R. Brandt¹
4 **Author Affiliations:**
5 ¹ Department of Energy Science & Engineering, Stanford University, Stanford, California 94305,
6 United States
7 ^a Present affiliation: Lawrence Berkeley National Laboratory, Berkeley, California, 94720,
8 United States
9 ^b Present affiliation: Highwood Emissions Management, Calgary, Alberta T2P 2V1, Canada
10 * Correspondence: evansherwin@lbl.gov

Deleted: ^a

Deleted: ^a

Deleted: Highwood Emissions Management, Calgary, Alberta T2P 2V1, Canada

Formatted: Not Superscript/ Subscript

Deleted: evands@stanford.edu

11

17 **Abstract**

18 Satellite-based remote sensing enables detection and mitigation of large point sources of climate-
19 warming methane. These satellites will have the greatest impact if stakeholders have a clear-eyed
20 assessment of their capabilities. We performed a single-blind test of nine methane-sensing
21 satellites from three continents and five countries, including both commercial and government
22 satellites. Over two months, we conducted 82 controlled methane releases during satellite
23 overpasses. Six teams analyzed the resulting data, producing 134 estimates of methane
24 emissions. Of these, 80 (58%) were correctly identified, with 46 true positive detections (34%)
25 and 34 true negative non-detections (25%). There were 41 false negatives, in which teams
26 missed a true emission, and 0 false positives, in which teams incorrectly claimed methane was
27 present. All eight satellites that were given a nonzero emission detected methane at least once,
28 including the first single-blind evaluation of the EnMAP, Gaofen 5, and Ziyuan 1 systems. In
29 percent terms, quantification error across all satellites and teams is similar to aircraft-based
30 methane remote sensing systems, with 55% of mean estimates falling within $\pm 50\%$ of the
31 metered value. Although teams correctly detected emissions as low as 0.03 metric tons of
32 methane per hour, it is unclear whether detection performance in this test is representative of
33 real-world field performance. Full retrieval fields submitted by all teams suggest that in some
34 cases it may be difficult to distinguish true emissions from background artifacts without a known
35 source location. Cloud interference is significant and appears to vary across teams and satellites.
36 This work confirms the basic efficacy of the tested satellite systems in detecting and quantifying
37 methane, providing additional insight into detection limits and informing experimental design for
38 future satellite-focused controlled methane release testing campaigns.

39
40 **Keywords:**

41 Methane, hyperspectral imaging, remote sensing, satellite, single-blind, controlled release

42
43 Satellite-based remote sensing systems continue to find large point-source emissions of climate-
44 warming methane across the globe (Lauvaux et al., 2022; Irakulis-Loitxate et al., 2022a, b;
45 Pandey et al., 2019; Varon et al., 2018, 2019, 2021; Sánchez-García et al., 2022). Such systems
46 empower stakeholders in industry and government to take corrective action, both to mitigate
47 individual sources and to inform estimates of total methane emissions, particularly in oil and
48 natural gas systems, where many of the largest sources have been observed (Lauvaux et al.,
49 2022; Irakulis-Loitxate et al., 2022a; Pandey et al., 2019; Varon et al., 2018; Irakulis-Loitxate et
50 al., 2022b; Varon et al., 2021, 2019; Cusworth et al., 2022; Duren et al., 2019; Chen et al., 2022;
51 Sherwin et al., 2023a; Sánchez-García et al., 2022).

52
53 A considerable fleet of point-source methane-sensing satellites is now in orbit, including
54 purpose-built and repurposed instruments (Jacob et al., 2022). In the coming years, this number
55 will increase substantially (Jacob et al., 2022).

56
57 These satellites will have the greatest positive environmental impact if their results are widely
58 believed by a broad array of stakeholders across the world. Single-blind controlled methane
59 release testing, in which teams estimate methane emissions from one or more metered sources
60 without knowing the true rate, is an important and widely-used method of independently
61 determining the capabilities of a methane sensing system (Sherwin et al., 2021, 2023b; Bell et
62 al., 2020, 2022, 2023; Ravikumar et al., 2019; Rutherford et al., 2023).

Deleted: a

Deleted: value

65
66 In the first such single-blind release testing satellite systems, Sherwin et al. tested five satellites:
67 the commercial GHGSat-C and WorldView-3 systems and the government-supported PRISMA,
68 LandSat 8, and Sentinel-2 systems. In that study five teams analyzed data from different subsets
69 of these satellites (Sherwin et al., 2023b). This test demonstrated that, across the array of these
70 five satellites, this approach can be used to detect emissions ranging from 0.20 [95% confidence
71 interval = 0.19, 0.21] metric tons of methane per hour (henceforth t/h), for the most sensitive
72 systems, to 7.2 [6.8, 7.6] t/h. Relative quantification error was comparable to aircraft-based
73 methane sensing systems, although with significantly larger detection limits (Sherwin et al.,
74 2023b). Sample size was modest, however, with some satellites collecting only one
75 measurement, limiting generalizability of the results without additional data collection.
76

77 In addition, several methane-sensing satellites have launched since the previous test concluded in
78 2021, including the German EnMAP system and the 02 edition of the Chinese Gaofen 5
79 Advanced Hyperspectral Imager (GF5) and the 02E edition of the Ziyuan 1_{Advanced}
80 Hyperspectral Imager (ZY1) (EnMAP, 2023; Xinhua, 2022; Song et al., 2022). Although these
81 satellites were not primarily designed to sense methane, scientists have used similar systems to
82 detect substantial methane point sources from oil and natural gas infrastructure (Irakulis-Loitxate
83 et al., 2021).
84

85 This work conducts single-blind testing of nine distinct satellite systems, focusing on detection
86 and quantification performance for releases ranging from 0.03-1.6 t/h. In addition, we take steps
87 to evaluate the generalizability of our results through a highly transparent experimental design, in
88 which all teams submit full methane retrievals for the scene surrounding the release. This
89 approach provides insight into which identified methane emissions are unambiguously detected
90 and which might be difficult to distinguish from artifacts if the source location were not known.

91 **1 Materials and Methods**

92
93 We employed a fixed-location single-blind controlled methane release experimental design to
94 evaluate point-source methane sensing systems from October 10th to November 30th, 2022.
95 Participating teams were aware of the existence, timeframe, and precise location coordinates of
96 the test site. Teams were not informed during a given observation whether gas would be
97 released, nor of the size of released emissions. Teams were informed of an approximate upper
98 bound of 1.5 t/h. Teams were not given the precise configuration of Stanford equipment on the
99 ground, though large equipment may have been visible from space in some cases.
100

101 Metered controlled release volumes – including releases with zero volume – were retained by the
102 Stanford team and not given to teams until all estimates were submitted by all participants for all
103 stages of the test. Analysts estimated the presence and magnitude of methane emissions for each
104 overpass, with a reporting approach in compliance with the Advancing Development of
105 Emissions Detection (ADED) protocol for airplane and satellite systems (Zimmerle, 2022). More
106 information is provided in the Supporting Information (SI), Section S1.1.
107

108 We performed releases during overpasses of nine satellite constellations: the commercial
109 satellites GHGSat-C (GSC) of Canada and the US-based WorldView-3 (WV3), as well as

Deleted: -02

Deleted: -02E

Deleted: .

Deleted: -

114 publicly-funded satellites, including the German Environmental Mapping and Analysis Program
115 (EnMAP), the Chinese Gaofen 5 (GF5), Ziyuan 1 (ZY1), and Huanjing 2 (HJ2), the Italian
116 PRecursore IperSpettrale della Missione Applicativa (PRISMA), the US LandSat (LS) 8 and 9,
117 and the pan-European Sentinel-2 (ESA, 2022a, b, c; Jervis et al., 2021; OHBI, 2022; EnMAP,
118 2023; Liu et al., 2019; USGS, 2022; Song et al., 2022; Zhong et al., 2021). With the exception of
119 the GHGSat-C constellation, none of these satellites was explicitly designed for methane
120 sensing, but their data have instead been applied to this end. Analysis teams first attempted to
121 estimate emissions volumes using available data from satellites and wind reanalysis products. In
122 some cases, multiple teams assessed the same observation from an instrument, providing an
123 opportunity to empirically assess variability due to source quantification algorithms, which
124 participating teams were not required to release. See the SI, Section S3 for the details each team
125 elected to share about their algorithms.

126
127 These satellites range from high-sensitivity/narrow swath to low-sensitivity/large swath, as
128 illustrated in Table 1. Revisit time is also anticorrelated with instrument sensitivity. The
129 Sentinel-2 and LandSat 8/9 systems have estimated detection limits of roughly 1-5 t/h (Gorroño
130 et al., 2023), but each satellite in these constellations covers the bulk of the world's landmass
131 every 10-16 days with a swath of 185-290 km (USGS, 2022; ESA, 2021a). GHGSat, EnMAP,
132 GF5, PRISMA, WorldView-3, and ZY1 are targeted "point-and-shoot" systems, with higher
133 resolution but narrower swaths of 12-60 km (ESA, 2022a, b; Jervis et al., 2021; OHBI, 2022;
134 EnMAP, 2023; Liu et al., 2019; Song et al., 2022). Existing publicly available information does
135 not specify whether HJ2 is targeted or has global coverage, but its swath of 800 km suggests it is
136 capable of global coverage (Zhong et al., 2021). Pixel size also varies widely across satellites,
137 with most tested satellites ranging from 20-30 m square pixels, while HJ2 has 6 km square pixels
138 and WorldView-3 has highly sensitive 3.7 m square pixels. Spectral resolution varies as well
139 across the tested satellites, from 0.3 nm for GHGSat-C and 200 nm for Sentinel-2 and LandSat
140 8/9 (Jacob et al., 2022), discussed further in the SI, Section S2. See the SI, Section S2 for
141 additional discussion of the capabilities of each satellite system.

Formatted: Font: 12 pt

Formatted: Font: 12 pt

Deleted: (Jacob et al., 2022)

Formatted: Font: 12 pt

Deleted: S1

Deleted: ¶

Table 1. Key characteristics of each participating satellite constellation, from lowest to highest swath width, which is roughly proportional to an instrument's minimum methane detection limit. Global coverage refers to a configuration that passively covers most of Earth's surface over some number of orbits, while targeted coverage refers to a "point-and-shoot" instrument that must be pointed to a particular location. [Nadir pixel size is presented here](#). Constellation size includes only active satellites. [Accessing data from the GF5, ZY1, and HJ2 satellites requires permission from the Chinese government](#). Adapted with permission from (Sherwin et al., 2023b).

Satellite	Coverage	Constellation size	Swath [km]	Pixel size [m]	~Revisit time (per satellite)	Data availability	Source
GHGSat-C	Targeted	8 [§]	12	25x25	14 days	Commercial	(ESA, 2022a; Jervis et al., 2021)
WorldView-3	Targeted	1	13.1	3.7x3.7	1 day [‡]	Commercial	(ESA, 2022b)
PRISMA	Targeted	1	30	30x30	7 days	Public	(OHBI, 2022; ESA, 2012)
EnMAP	Targeted	1	30	30x30	4 days [†]	Public	(EnMAP, 2023)
Gaofen 5 (GF5)	Targeted	1	60	30x30	5-8 days [*]	Government	(Liu et al., 2019; Zhang et al., 2022; Luo et al., 2023)
Ziyuan 1 (ZY1)	Targeted	1	60	30x30	1-3 days [*]	Government	(Song et al., 2022)
Landsat 8/9	Global	2	185	30x30	16 days	Public	(USGS, 2022)
Sentinel-2	Global	2	290	20x20	10 days	Public	(ESA, 2021a)
Huanjing 2 (HJ2)	Unknown	2	800	6x6 km	≤4 days [*]	Government	(Zhong et al., 2021)

[§]Three of these GHGSat C satellites were launched after the conclusion of testing.

[‡]WorldView-3 requires a 4.5-day repetition cycle for best resolution within 20° off nadir.

[†]EnMAP requires a 27-day repetition cycle for best resolution within 30° off nadir (Jacob et al., 2022).

^{*}Revisit times for GF5, ZY1, and HJ2 are inferred, at least in part, from overpass schedules submitted by NJU.

Deleted: Sherwin et al. 2023

Formatted: Font: (Default) Times New Roman

Formatted Table

Deleted: 26,27

Formatted: Font: (Default) Times New Roman

Deleted: 28

Deleted: 4.5... days ... [1]

Formatted: Font: (Default) Times New Roman

Deleted: 29

Formatted: Font: (Default) Times New Roman

Formatted ... [2]

Deleted: 21

Formatted: Font: (Default) Times New Roman

Deleted: 27

Deleted: 30,37,38

Formatted: Font: (Default) Times New Roman

Deleted: 23

Formatted: Font: (Default) Times New Roman

Deleted: 31

Formatted: Font: (Default) Times New Roman

Deleted: 35

Formatted: Font: (Default) Times New Roman

Deleted: 33

Deleted: Global

Formatted: Font: (Default) Times New Roman

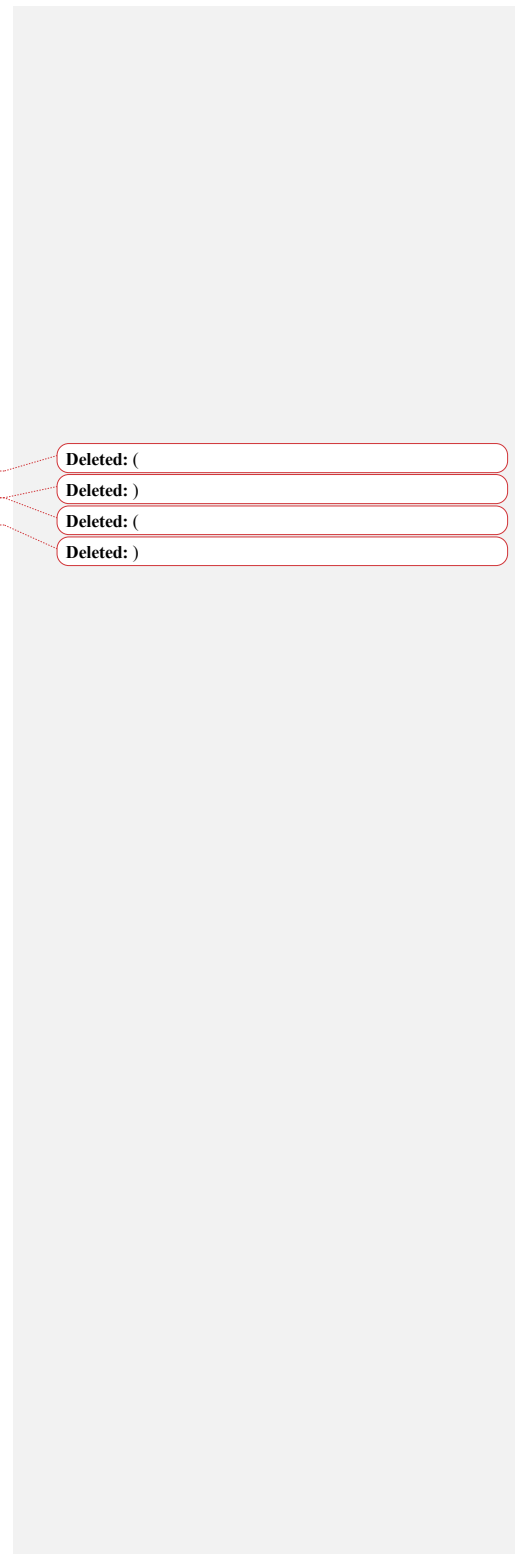
Deleted: F...orldView-3 requires a 4.5-day repetition cycle for best resolution within 20° off nadir....WorldView-3 has 1-day revisit time at lower guaranteed resolution. ... [3]

Deleted: For best resolution within 30° off nadir, EnMAP has 4-day revisit time at lower guaranteed resolution

1
2
3
4
5
6
7
8
9
10
11
12
13
14
15
16
17
18

This test does not include the TROPOMI system on the Sentinel-5P satellite, which has a detection limit far above the maximum of the release apparatus used in this study (ESA, 2021b). We inquired about tasking the Earth Surface Mineral Dust Source Investigation (EMIT) satellite, launched by the US National Aeronautics and Space Administration (NASA) in July 2022 (Wang and Lee, 2022), but the system was not available to participate in this test.

Participating analysis teams include private companies GHGSat (GHGSat, 2022), Kayros (Kayros, 2022), Maxar (Scott, 2022), and Orbio Earth (Orbio, 2023), as well as the Land and Atmosphere Remote Sensing (LARS) group of university researchers from Universitat Politècnica de València [Luis Guanter, Javier Roger Juan, and Javier Gorroño Viñegla (Irakulis-Loitxate et al., 2022a, b, 2021; Guanter et al., 2021)] and Nanjing University [Fei Li, Huilin Chen, and Yongguang Zhang (Jia et al., 2022)]. Each analysis team had the opportunity to submit estimates for all satellites tested, with the exception of the GHGSat-C satellites, to which GHGSat had sole access. See the SI, Section S3 for a description of each team and its members, as well as a list of invited teams that declined to participate.



Deleted: ()
Deleted:)
Deleted: ()
Deleted:)

23 **1.1 Materials**

24 For the full test period, our experimental equipment was located near Casa Grande, Arizona,
25 south of Phoenix, Arizona in the United States, with the release stacks located at [32.8218205°, -
26 111.7857730°].

27
28 The methane source was two trailers of compressed natural gas, shown in Figure 1, which passed
29 through a pressure regulation and reheating apparatus. The gas was then transmitted to the
30 metering and release trailer via a 7.62 cm (3 in) shipping hose at an exit pressure of roughly 150-
31 200 psig (1.03-1.37 Mpa), passing through one of three possible Coriolis meters before release
32 through one of two stacks, at a release height of either 7.3 or 3.0 m above ground level (El
33 Abbadi et al., 2023), shown in the SI, Figure 1. This testing setup approximately mimics an unlit
34 flare or tank vent on an oil and gas production site or other facility.

Deleted: n
Deleted: "



38
39 Figure 1. Aerial photograph of the site. Note that the workstation is ~60 m from the release apparatus and ~50m
40 from the compressed natural gas (CNG) trailers. Reproduced with permission from (El Abbadi et al., 2023).

Deleted: El Abbadi et al.
Formatted: Font: 10 pt

41 This experiment was designed to provide near-optimal conditions for methane-sensing satellites.
42 In addition to the desert background, the site contained only equipment necessary to conduct
43 controlled methane releases and test a suite of methane sensing technologies. The result is a

47 significantly less complex scene than many oil and gas facilities, which will often contain
48 multiple pieces of infrastructure such as wellheads, tanks, flares, and separators at production
49 sites, and entire buildings with sophisticated machinery and piping at compressor stations and
50 gas processing plants. More complex scenery can make methane remote sensing more
51 challenging. Future work with scenes that more closely mimic industrial sites will help determine
52 the associated differences in technology efficacy, if any.

54 Achievable release rates for the three Coriolis meters, installed in pipes of different diameter,
55 were 2 – 30 kilograms per hour (kg/h), 30 – 300 kg/h, and 300 – 2,000 kg/h for natural gas. See
56 (El Abbadi et al., 2023) for further detail.

Deleted: El Abbadi et al. 2023

Deleted: (El Abbadi et al., 2023)

58 1.2 Safety

59 All natural gas equipment fabrication, operation, and transportation was conducted by personnel
60 affiliated with Rawhide Leasing, a gas services contractor. Stanford personnel contributed to
61 assembly of some equipment, but did not operate natural gas release equipment or pass within
62 our 100-foot (30.5 m) safety perimeter fence during active releases. The research workstation,
63 from which Stanford researchers coordinated data collection and related field operations, was
64 ~60 m away from any equipment through which natural gas flowed.

66 In addition, Stanford researchers periodically monitored plume dissipation in real time via a
67 FLIR GasFinder 320 infrared camera and continuously paid attention to olfactory signals from
68 the gas, which was odorized. The infrared camera showed clearly that the plume dissipated well
69 before reaching any on-site personnel. Equipment design contributed to this intrinsic safety,
70 because the emission source was elevated off the ground and gas often exited at a high vertical
71 velocity, particularly at larger release volumes, accelerating natural methane lofting. When
72 Stanford researchers detected gas smell during testing, they diligently checked infrared footage
73 of the plume and/or ambient wind conditions to ensure safety of all personnel onsite.

75 1.3 Data logging

76 Stanford researchers collected data logs directly from the Coriolis gas flow meters, accounting
77 for modest timestamp offsets as described in (El Abbadi et al., 2023).

Deleted: El Abbadi et al. 2023

79 1.4 Data collection procedures

80 All satellite-coincident releases began at least 15 minutes before the scheduled satellite overpass
81 time, provided by participating teams.

83 Stanford personnel set all release levels remotely, using WiFi-enabled control software deployed
84 on a laptop computer. For releases conducted on or before October 20th, Stanford personnel set a
85 desired flow rate, with an automated control system adjusting valves in real-time to target that
86 rate. After it became clear that this approach resulted in unnecessary flow rate variability,
87 releases from October 21st on were conducted by setting the relevant valve to a desired level of
88 openness, improving flow stability while slightly reducing the system's ability to target a specific
89 release rate, although this system still represents a major improvement over the manual approach
90 employed in (Sherwin et al., 2023b). Flow can fluctuate during the releases due to shifts in
91 pressure, temperature, and simple turbulent flow through the system. All performed releases

Deleted: (

Deleted: Sherwin et al. 2023

Deleted:)

98 except four had flow variability with a 5-minute 95% confidence interval within $\pm 10\%$ of mean
99 flow. On November 15th, a GF5 satellite acquisition was rescheduled without notice to the
100 Stanford team for a time that happened to be one minute after conclusion of a different satellite
101 release, resulting in flow variability within $\pm 20\%$ of the 5-minute mean. Three additional
102 releases exceeded a 5-minute flow variability 95% confidence interval of $\pm 10\%$: the October 11th
103 GHGSat-C overpass (in which the instrument was not tasked), the October 17th WorldView-3
104 release of 0.042 [0.034, 0.050] t/h, and the November 30th PRISMA release of 0.98 [0.87, 1.08]
105 t/h.

Formatted: Superscript

106
107 Interference from other sources was examined and found to be minimal. Over the course of the
108 experiment, we tested the Carbon Mapper, GHGSat AV, Kairos Aerospace, MethaneAIR, and
109 Scientific Aviation aerial methane sensing systems (El Abbadi et al., 2023), all of which are
110 more sensitive than any of the satellites tested. These aircraft, which also surveyed the nearby
111 area during the process of data collection, found no detectable methane sources outside our test
112 site. This strongly suggests that our test was free of interference from significant confounding
113 methane sources. The only evidence of modest possible landfill interference comes Scientific
114 Aviation, whose highly sensitive in situ measurement technology found modest and diffuse
115 methane concentration enhancements over a nearby landfill, potentially impacting only one of
116 the three days of testing, and only one of the seven measurements conducted on that day (El
117 Abbadi et al., 2023).

119 1.5 Flow rate uncertainty

120 Sources of uncertainty in measured methane flow rates include variability in actual natural gas
121 flow rates (represented as the standard deviation of metered natural gas flow over a 5-minute
122 period), rated meter uncertainty, and uncertainty in gas composition, which can vary even for a
123 consistent supplier. We used highly precise Coriolis meters, which have manufacturer rated
124 uncertainty of 0.25% of the flow rates used in this study (El Abbadi et al., 2023). Natural gas
125 composition for the gas used in these releases, derived from measurement stations on the
126 transmission pipeline that supplied the gas used in this test, ranged between 93.6% [93.3%,
127 93.9%] and 95.4% [94.7%, 96.1%] methane, described further in the SI, Section S1.2 and in
128 reference (El Abbadi et al., 2023). We propagate these sources of error into our metered values
129 using code listed in data and code availability statement. See (El Abbadi et al., 2023) for further
130 discussion of sources of metering uncertainty and our method of determining flow rate
131 uncertainty, as well as detailed gas composition data.

Deleted: El Abbadi et al. 2023

Deleted: (El Abbadi et al., 2023)

132
133 Following (Sherwin et al., 2023b), we use a 5-minute averaging period used to compute flow
134 variability. This is based on the fact that a plume traveling with a relatively slow average wind
135 speed of 2 m/s, the minimum observed 5-minute average wind speed for any valid satellite
136 measurement, would traverse 600 m within 5 minutes (300 seconds). By this distance, much of
137 the originally emitted methane has likely dissipated into background concentrations, with the
138 bulk of the methane enhancement detected by a satellite remaining closer to the release point.
139

Deleted: Sherwin et al. 2023

Deleted: (Sherwin et al., 2023b)

140 1.6 Experimental design

141 This single-blind field trial employed a two-stage experimental design, modeled on (Sherwin et
142 al., 2023b). This approach aims to disentangle the effect of wind speed uncertainty from other
143 sources of methane quantification uncertainty, e.g. due to algorithmic differences.

Deleted: Sherwin et al. 2023

149
150 Stanford personnel released metered quantities of methane from the test site via procedures
151 described above and in reference (El Abbadi et al., 2023). The Stanford ground team and
152 contract personnel operating equipment communicated no information to participating teams
153 regarding metered flow rates or metered wind speed or direction. Participating teams were aware
154 of the precise location coordinates of the test, but were not informed of the precise configuration
155 of ground-based equipment within the test site. Teams were given a rough range of possible
156 overall flow rates, from below 0.01 t/h to roughly 1.5 t/h. To facilitate efficient tasking of
157 government satellites, LARS and NJU were informed in advance that weekend releases in
158 November would be cancelled and all such dates were excluded from single-blind analysis for
159 those teams. In addition, participating teams were not informed of the details of the equipment or
160 its configuration, or the diameter of the pipes and hoses involved, although teams were informed
161 that the test would use compressed natural gas as the methane source.

162
163 After each team submitted final stage 1 estimates based on the above information, we proceeded
164 to stage 2 estimates. In stage 2, Stanford provided 10 m wind speed and direction data from our
165 on-site ultrasonic anemometer (shown in Figure 1) at one-second resolution and teams were
166 allowed to re-estimate emissions based on measured ground wind conditions rather than re-
167 analysis products as in stage 1. All teams submitted stage 1 and stage 2 estimates, with the
168 respective timelines described in the SI, Section S2.10. Note that turnaround time for results in
169 this study may not be representative of commercial or field performance.
170

Deleted: ,

Deleted: or

Deleted: location

174

175 **2 All tested satellites detected methane**

176

177 For the eight satellites given nonzero methane emissions, at least one analysis team correctly
178 detected methane. The single HJ2 measurement, using the HJ2B satellite, was rescheduled
179 without notice to a time in which Stanford was not releasing methane.

180

181 In total, the nine tested satellites conducted 82 overpasses. Six analysis teams analyzed data from
182 between 1 – 8 satellites each, resulting in a total of 492 potential estimates. Stanford filtered
183 many of these estimates from analysis before teams submitted results, for various reasons (e.g.
184 due to release system malfunction or prior notice to teams tasking government satellites that
185 there would be no weekend releases in November). In addition, most teams opted to submit
186 estimates for only a subset of all available satellites. See the SI, Section S1.3 for further
187 discussion of data exclusion criteria.

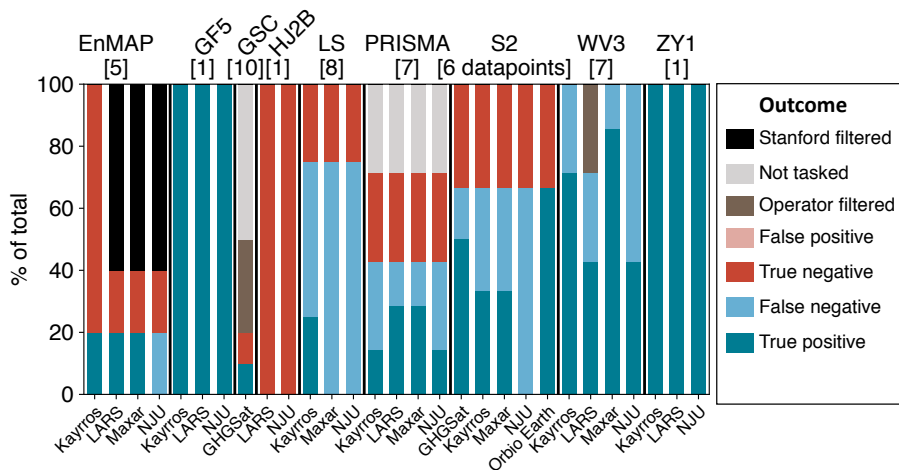
188

189 Of the 139 estimates not filtered by Stanford, in five instances (3.6% of the total), teams filtered
190 estimates using internal quality control criteria related to cloud cover, image clipping, or other
191 factors that could compromise the ability to produce a valid methane estimate. GHGSat filtered
192 three retrievals from the GHGSat-C satellite due to clouds (see Figure 8 and the SI, Section S4
193 for sky images and further discussion of clouds). LARS filtered two WorldView-3 retrievals due
194 to cloud cover (November 22th) and inconsistent wind, and possible effects of human-made
195 surface features (October 10th). As a result, a total of 134 estimates included valid methane
196 detection estimates.

197

198 Of these 134 estimates, 80 (58%) were identified as either a true positive or true negative,
199 correctly determining the presence or absence of methane, as shown in Figure 2. True positives
200 represent 46 (34%) of total estimates with valid detection estimates, with 34 (25%) true
201 negatives. Note that for Sentinel-2, we consider non-detection of an 0.005 t/hr release on
202 November 28th to be a true negative, as this value is more than two orders of magnitude below
203 existing estimates of the detection threshold of this system (Gorroño et al., 2023; Sherwin et al.,
204 2023b).

205



207 Figure 2. Detection performance by satellite and team. The total number of measurements per satellite is listed in
 208 brackets, excluding measurements filtered by Stanford across all teams. All teams analyzing data from the three
 209 Chinese satellites, Gaofen 5 Advanced Hyperspectral Imager (GF5), Ziyuan 1 (ZY1), and Huanjing 2B (HJ2B) all
 210 correctly classified all emissions. Detection performance varied substantially across the Sentinel-2 (S2) and LandSat
 211 8/9 (LS) wide-area satellites. On several days, anticipated measurements from PRISMA and GHGSat-C (GSC) were
 212 not collected because the satellite was not tasked. In others, e.g. two WorldView-3 retrievals from LARS, no
 213 retrieval was conducted due to concerns over image clipping or excessive cloud cover. No teams submitted false
 214 positives, in which they reported the presence of methane when none was released.
 215

216 Of the 41 false negatives (30%), most (25) are concentrated in the lower-sensitivity Sentinel-2
 217 and LandSat 8/9 systems. There is substantial variability in false negative rates across teams. For
 218 example, Orbio Earth correctly classifying all valid Sentinel-2 releases. GHGSat missed only one
 219 Sentinel-2 release, and NUJ detected none. This highlights that analysis of identical spectral data
 220 can produce very different results. As in (Sherwin et al., 2023b), there were no false positives,
 221 defined as incorrect reports of the presence of methane,
 222

223 In several cases, a satellite was not tasked during an overpass for which the Stanford team
 224 conducted a release, either due to technical issues, scheduling issues, or miscommunications
 225 between the Stanford team and the operator. This occurred for five GHGSat overpasses and two
 226 PRISMA overpasses, resulting in a total of 13 Not Tasked estimates from participating teams for
 227 these two satellites, 9% of all estimates not filtered by Stanford.
 228

229 **2.1 First-time single-blind detections from three satellites**

230 This work includes the first-ever single-blind test of the Chinese Ziyuan 1 (ZY1), Gaofen 5
 231 (GF5), and Huanjing 2B satellites (HJ2B), as well as the European EnMAP satellite. Previous
 232 studies have used a subset of these satellites to detect and quantify point-source emissions with
 233 estimated magnitudes as small as 0.5 t/h, but have not performed ground-truth testing (Irakulis-
 234 Loitxate et al., 2021). Roger et al. compare EnMAP retrievals with the single-blind-validated

Deleted: -02

Deleted: Sherwin et al. 2023

Deleted: (Sherwin et al., 2023b)

Deleted: Chinese and European

PRISMA satellite as a benchmark, finding promising results, especially for offshore emissions of 1 t/h or more (Roger et al., 2023).

Figure 3 shows masked methane plume images from ZY1, GF5, and EnMAP, over a standard optical satellite image background, for emissions of roughly 1 t/h. Masking refers to the process of spatially differentiating a methane emission from background noise. The HJ2B acquisition was rescheduled without prior notice to the Stanford team to a time at which no release took place, which all teams analyzing HJ2B data correctly identified as a non-emission. We present images from all teams analyzing satellite data from these measurements, including LARS, Kayrros, NJU, and Maxar. See the SI, Section S4 for masked and unmasked plume images for all satellites and teams.

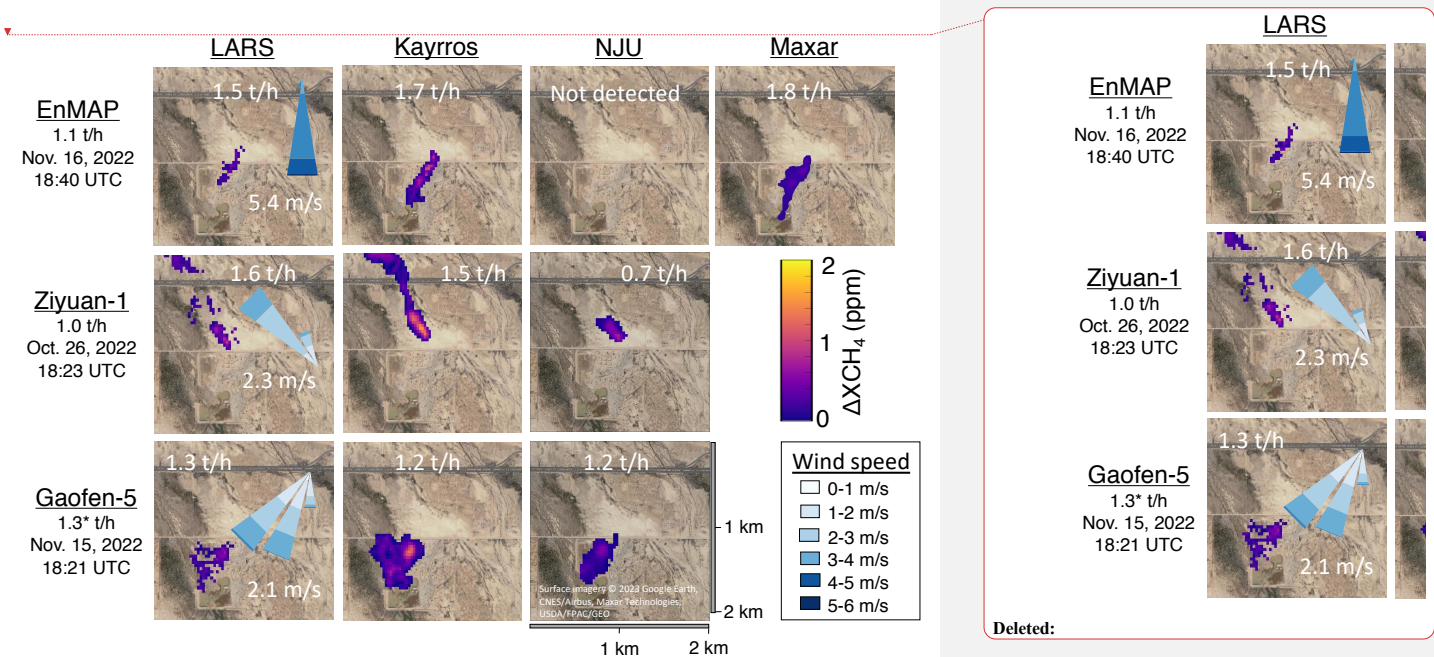


Figure 3. Visualization of detected emissions for the newly-tested European and Chinese satellites, using the release closest to 1 t/h in all cases. The true measured emission rate, as well as the timestamp are shown below the satellite name. Mean estimated volume from each team/satellite pair, as well as a 5-minute wind rose of measured 10-meter wind speed and the direction toward which the wind was blowing, are superimposed on the corresponding picture. The wind rose represents a histogram of one-second wind measurements in each direction, broken down by wind speed. Where an emission was not detected, we show the full unmasked retrieval field. Cloud-free surface imagery © 2023 Google Earth, CNES/Airbus, Maxar Technologies, USDA/FPAC/GEO. ~~The Gaofen 5 measurement was rescheduled without notice to a time that happened to be one minute after releases had concluded for a different satellite, resulting in artificially high variability in the metered ground-truth flow rate.~~

Note that, as was observed in (Sherwin et al., 2023b), teams analyzing precisely the same spectral data can produce methane plume masks with very different shapes. Each row represents

- Formatted: Superscript
- Formatted: Not Superscript/ Subscript
- Deleted: Sherwin et al. 2023
- Deleted: (Sherwin et al., 2023b)

267 a distinct satellite, while each column shows estimates from a distinct team. For example, the
268 first row shows estimates for the November 16th EnMAP satellite measurement, for which four
269 teams submitted estimates. Three of the four teams detected the emission. LARS, Kayrros, and
270 Maxar all show masked plumes traveling in roughly the same direction, but the Kayrros and
271 Maxar plumes are fairly contiguous, while the LARS plume is smaller and contains disjunct or
272 tenuously-connected clusters of estimated methane enhancements. Overall, masks from LARS
273 are more conservative and less spatially contiguous than other teams. However, quantification
274 estimates from LARS, Kayrros, and Maxar all have overlapping quantification intervals,
275 demonstrating that the results are not statistically distinguishable across these three teams (NJU
276 did not detect this EnMAP emission). Even with cases with large mean differences, e.g. October
277 26th estimates for ZY1, which range from 1.6 [1.2, 2.0] t/h for LARS to 0.7 [0.6, 0.9] t/h for
278 NJU, the 95% confidence intervals overlap. These findings suggest that many factors influence
279 quantification performance, even when working with identical spectral data, but large
280 uncertainties make disentangling these differences a challenge. Further analysis of these
281 algorithmic differences is beyond the scope of this work, as teams were not asked to provide
282 algorithmic details, which are often proprietary. Further experimentation may enable analysis of
283 general trends in advantages of one algorithm over another, but the order-100 number of
284 datapoints here is insufficient to make such judgements.

285
286 Wind can vary substantially in speed and direction even on five-minute timescales relevant to
287 methane quantification, as shown in wind roses inset in the left-most panel for each satellite in
288 Figure 3. This variability clearly influences plume formation, with emissions with steadier wind
289 directions and higher speed, such as the EnMAP and ZY1 measurements shown here (5.4 [3.7,
290 7.2] m/s and 2.3 [1.0, 3.7] m/s average wind speed, with a wind direction circular standard
291 deviation of 16° and 11°, respectively), resulting in narrower plumes. The highlighted GF5
292 measurement has slower and more variable winds and a wider plume in all three retrievals (2.1
293 [0.3, 4.0] m/s, with a wind direction circular standard deviation of 18°).

295 **2.2 Reliable overall quantification performance**

297 Releases in this study covered a wide range of emission rates, as low as 0.0332 [0.0328, 0.0336]
298 t/h, analogous to a medium-sized liquids unloading event at an oil and gas production site (Bell
299 et al., 2017), and as high as 1.48 [1.43, 1.52] t/h, analogous to a medium-sized unlit flare
300 (Cusworth et al., 2021). For all detected emissions, mean estimates for all satellite-team
301 combinations are between -56% and 456% of the metered value (Figure 4; see also SI, Section
302 S5), with 55% of nonzero estimates falling within ±50% of the metered value. Excluding
303 estimates from Maxar, which discovered after submitting results that its estimates were likely a
304 factor of 2.3 too high due to a misinterpretation of a deprecated spectral absorption library, this
305 fraction rises to 63% (Hayden and Christy, 2023). However, the best-fit line across all satellite
306 measurements, any one of which may have substantial quantification error, is largely unbiased,
307 with a slope close to the ideal value of 1 (which would denote perfect agreement on average).

Deleted: Q

Deleted: approaches aircraft-level accuracy

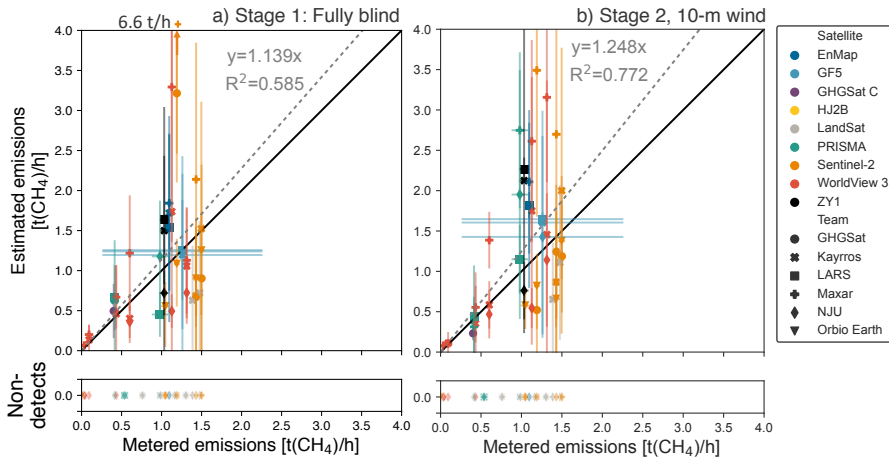
Deleted: Figure 4

Moved down [2]: The latter overall performance approaches that of the satellites and teams tested in Sherwin et al. 2023, in which 75% of estimates fell within ±50% of the metered value, demonstrating a relative error profile similar to that observed in aircraft-based methane remote sensing technologies¹⁴. Direct comparison with the results in Sherwin et al. 2023 is complicated by the fact that releases in this study focused on smaller emissions, with a maximum of roughly 1.5 t/h instead of 7.2 t/h. Aircraft-based methane remote sensing technologies tested in El Abbadi et al. tend to have modestly better quantification performance in percentage terms, with 68-80% of estimates from Carbon Mapper, GHGSat, Kairos Aerospace, and MethaneAIR falling within ±50% of the metered value⁴⁷, a substantial improvement over prior tests of the same technologies^{18,51}.

See the SI, Section S4 for error summary statistics by satellite and team. Error bars in metered values along the x-axis are generally too small to be visible, with the notable exception of the GF5 measurement, which was rescheduled without notice to a time that happened to be one minute after releases had concluded for a different satellite.

Deleted: The latter overall performance approaches that of that of the satellites and teams tested in Sherwin et al. 2023, in which 75% of estimates fell within ±50% of the metered value, demonstrating a relative error profile similar to that observed in aircraft-based methane remote sensing technologies¹⁴. Direct comparison with the results in Sherwin et al. 2023 is complicated by the fact that releases in this study focused on smaller emissions, with a maximum of roughly 1.5 t/h instead of 7.2 t/h. Aircraft-based methane remote sensing technologies tested in El Abbadi et al. tend to have modestly better quantification performance in percentage terms, with 68-80% of estimates from Carbon Mapper, GHGSat, Kairos Aerospace, and MethaneAIR falling within ±50% of the metered value⁴⁷, a substantial improvement over prior tests of the same technologies^{18,51}.

See the SI, Section S4 for error summary statistics by satellite and team. Error bars in metered values along the x-axis are generally too small to be visible, with the notable exception of the GF5 measurement, which was rescheduled without notice to a time that happened to be one minute after releases had concluded for a different satellite.



358 Figure 4. Methane quantification performance by satellite and team. Metered emissions compared with single-blind
 359 estimates for each overpass with successfully reported data, with 95% X and Y confidence intervals. a) Fully blind
 360 stage 1 results using modeled wind speed estimates. Note one Sentinel-2 estimate exceeds the y-axis limit at 6.6
 361 t(CH₄)/h. b) Stage 2 results using on-site 10 m wind speed and direction measurements. LARS WorldView-3
 362 quantification estimates are excluded from the main analysis, as stage 1 estimates were submitted after wind data
 363 had been unblinded to a member of the LARS team not involved in analyzing WorldView-3 data, while
 364 corresponding stage 2 estimates were submitted after release volumes were unblinded. Note that Maxar submitted
 365 PRISMA estimates for stage 2 only. The grey dashed lines represent an ordinary least squares fit with the intercept
 366 fixed at zero, with slope and uncentered R² displayed. Maxar has since determined that its estimates were likely
 367 artificially high, potentially introducing upward bias into aggregate statistics (Hayden and Christy, 2023). See the SI,
 368 Section S4.2 for a version of this plot excluding Maxar, which shows overall improvement in both slope and R². The
 369 black solid lines denote exact 1:1 agreement. See the SI, Section S4 for satellite- and team-specific results.

371 In percent quantification error terms, this overall performance approaches that of the satellites
 372 and teams tested in Sherwin et al. 2023, in which 75% of estimates fell within ±50% of the
 373 metered value, demonstrating a relative error profile similar to that observed in aircraft-based
 374 methane remote sensing technologies (albeit with minimum detection limits one to three orders
 375 of magnitude larger) (Sherwin et al., 2023b; El Abbadi et al., 2023; Bell et al., 2022). Direct
 376 comparison with the results in Sherwin et al. 2023 is complicated by the fact that releases in this
 377 study focused on smaller emissions, with a maximum of roughly 1.5 t/h instead of 7.2 t/h.
 378 Aircraft-based methane remote sensing technologies tested in El Abbadi et al. tend to have
 379 modestly better quantification performance in percentage terms, with 68-80% of estimates from
 380 Carbon Mapper, GHGSat, Kairos Aerospace, and MethaneAIR falling within ±50% of the
 381 metered value (El Abbadi et al., 2023), a substantial improvement over prior tests of the same
 382 technologies (Sherwin et al., 2021; Rutherford et al., 2023). In each of these cases, best-fit lines
 383 have a slope that is similarly close to 1:1 agreement.

384
 385 See the SI, Section S4 for error summary statistics by satellite and team. Error bars in metered
 386 values along the x-axis are generally too small to be visible, with the notable exception of the

Formatted: Superscript

Moved (insertion) [2]

Deleted: The latter

Deleted:

389 GF5 measurement, which was rescheduled without notice to a time that happened to be one
390 minute after releases had concluded for a different satellite.

Deleted: ¶

392 In stage 2 of the test, teams produced updated results using measured 10 m wind data from an
393 on-site three-dimensional ultrasonic anemometer, though still blind to released volumes.
394 Applying an ordinary least squares linear fit to all quantified emissions, with the intercept set to
395 zero, we see a modest increase in slope, rising from 1.139 [0.832, 1.446] in stage 1 to 1.248
396 [1.037, 1.459] in stage 2 (Figure 4).

Deleted: Figure 4

397
398 Interpretation of these results is complicated by the fact that the Maxar team discovered after
399 submitting blinded results that the spectral library underlying their estimates contained an error
400 that likely artificially inflated their estimates by a factor of 2.3, discussed in detail in a white
401 paper produced by Maxar personnel (Hayden and Christy, 2023). This is consistent with the
402 Maxar-specific parity chart in the SI, Section S4, alongside other satellite- and team-specific
403 results, which shows a regression best fit line of 2.334 [1.030, 3.638] and an uncentered R^2 of
404 0.96, indicating a close linear fit. Excluding Maxar results (as in the SI, Section S4.2), the Stage
405 1 slope for all remaining teams falls to 0.897 [0.716, 1.078], with a Stage 2 slope of 1.010
406 [0.841, 1.180], almost perfect average agreement with metered values. These slopes are 21% and
407 19% below the respective estimates in which Maxar values were included.

408
409 Note that LARS WorldView-3 quantification estimates are excluded from the main analysis, as
410 stage 1 estimates were submitted after wind data had been unblinded to a member of the LARS
411 team not involved in analyzing WorldView-3 data, while corresponding stage 2 estimates were
412 submitted after release volumes were unblinded. Although the Stanford team believes all LARS
413 quantification estimates for WorldView-3 were submitted without leveraging unblinded data, we
414 must exclude them from the main analysis. This does not affect the integrity of detection
415 estimates, as only wind measurements were unblinded when these were first submitted. See the
416 SI, Section S4 for LARS WorldView-3 quantification results.

417
418 After incorporating on-site wind measurements, the uncentered R^2 increases from 0.585 to 0.772,
419 a substantial improvement in goodness-of-fit. Excluding Maxar results, these numbers rise to
420 0.768 and 0.826, respectively. The linear fit presented here treats all estimated emission rates
421 from all team as independent datapoints. Note that uncentered R^2 values from such a linear fit,
422 with a zero intercept, have a different interpretation than R^2 values from nonzero-intercept
423 regressions and should not be compared directly. See (Sherwin et al., 2023b), SI Section S5 for
424 further explanation of the reasons for an ordinary least squares fit with the intercept fixed to zero.
425 This improved average linear fit with in situ wind does not necessarily translate to lower error for
426 each individual satellite, as shown in the SI, Section S4, alongside additional regression results.

Deleted: Sherwin et al. 2023

Deleted: (Sherwin et al., 2023b)

427
428 Confidence intervals submitted by teams appear to be modestly overconfident. For Stage 1
429 estimates, the metered value is within the provided 95% confidence interval only 70% of the
430 time, somewhat below the expected value of 95% for perfectly-calibrated 95% confidence
431 intervals. For Stage 2, this fraction falls to 52%, although mean error improves. Note that these
432 values combine results from multiple satellites and teams, and thus represent an overall sense of
433 the performance of satellite-based methane sensing systems as a technology class. Additional
434 data collection is needed to characterize the performance of each individual satellite in detail.

439
440
441
442
443
444
445
446
447
448
449
450
451

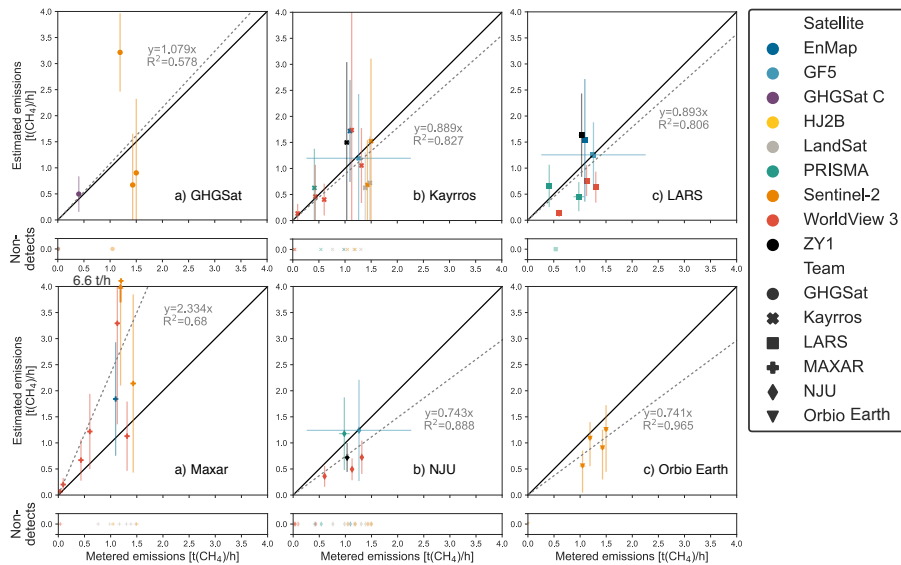
Figure 5 shows Stage 1 fully blinded results, the same underlying data as in [Figure 4](#), for each individual team. Team-specific parity lines tend to fall near the ideal 1:1 level, with Orbio Earth and NJU exhibiting modest low bias parity slopes of 0.74. Note that Maxar’s parity slope of 2.3 matches almost exactly with the factor of 2.3 they believe was error introduced into their system through misinterpretation of a deprecated spectral library (Hayden and Christy, 2023). The bulk of false negatives were from the relatively low-resolution Sentinel-2 and LandSat 8/9 satellites. However, Orbio Earth successfully detected all Sentinel-2 releases, [except a release below 0.010 t/h \(testing another technology\), far below all estimates of the Sentinel-2 detection limit](#) (Gorroño et al., 2023; Sherwin et al., 2023b). [These results highlight algorithmic variation across](#) teams analyzing the same spectral data.

Deleted: Figure 4

Deleted: above

Deleted: ,

Deleted: ing



456
 457 Figure 5. Parity charts by team, for fully blinded Stage 1 estimates only. Metered emissions compared with single-
 458 blind estimates for each overpass with successfully reported data, with 95% X and Y confidence intervals. Note one
 459 Maxar Sentinel-2 estimate exceeds the y-axis limit at 6.6 t(CH₄)/h. LARS stage 1 WorldView-3 quantification
 460 estimates are excluded from the main analysis, as they were submitted after wind data had been unblinded to a
 461 member of the LARS team not involved in analyzing WorldView-3 data. The grey dashed lines represent an
 462 ordinary least squares fit with the intercept fixed at zero, with slope and uncentered R² displayed. Maxar has since
 463 determined that its estimates were likely artificially high, potentially introducing upward bias into aggregate
 464 statistics (Hayden and Christy, 2023). The black solid lines denote exact 1:1 agreement. See the SI, Section S4 for
 465 Stage 1 and Stage 2 satellite- and team-specific results.

466
 467 **2.3 Qualitatively assessing detection performance in the field**

468 The smallest emission detected by each team gives a rough upper bound on the lower detection
 469 capabilities of each instrument, at least in a desert environment with a known release location.
 470 We compare these smallest detected emissions with previous estimates of lower detection
 471 capabilities of each satellite. The smallest emission detected was 0.0332 [0.0328, 0.0336] t/h,
 472 identified by Maxar using WorldView-3, shown in Figure 6. Kayros also detected an emission
 473 below 0.1 t/h using WorldView-3. This is consistent with previous estimates of lower detection
 474 capabilities, with Sánchez-García et al. detecting an emission estimated at ~0.040 t/hr in
 475 Turkmenistan using WorldView-3 (Sánchez-García et al., 2022).

476
 477
 478 Orbio Earth, Maxar, and GHGSat all detected a 1.19 [1.15, 1.23] t/h emission using Sentinel-2,
 479 with errors ranging from -8% to +170%. Orbio Earth detected a 1.05 [0.99, 1.10] t/h emission to
 480 within ±47%. These emissions are 15-25% below the smallest emission detected using Sentinel-
 481 2 in any previous satellite controlled methane release test, and consistent with simulation-based

Deleted: sense of
 Deleted: minimum

Deleted: than

485 estimates (Sherwin et al., 2023b; Gorroño et al., 2023). The story is similar for LandSat 8/9, with
486 the smallest detected emission at 1.39 [1.34, 1.43] t/h. This is also slightly below estimated lower
487 detection capabilities in the literature (Jacob et al., 2022).

488
489 The smallest emission detected via PRISMA was 0.414 [0.410, 0.417] t/h smaller than the 0.5-
490 2.0 t/h estimated by Guanter et al. as PRISMA's lower detection threshold (Guanter et al., 2021).
491 The smallest detected emissions for the remaining satellites are 1.10 [1.06, 1.13] t/h for EnMAP,
492 1.26 [0.26, 2.26] t/h for GF5, and 1.03 [0.98, 1.09] t/h for ZY1. However, given that the
493 technical characteristics of these three satellites are similar to PRISMA, they can likely be used
494 to detect emissions below 1 t/h, at least under favorable environmental conditions (Jacob et al.,
495 2022; Roger et al., 2023).

496
497 GHGSat correctly detected and quantified the only nonzero release for which GHGSat-C
498 collected data and passed quality control, which was 0.401 [0.399, 0.404] t/h, roughly double the
499 smallest release GHGSat quantified using the same satellite system in (Sherwin et al., 2023b).
500 GHGSat's lower detection threshold is estimated at 0.1-0.2 t/h (Jacob et al., 2022). HJ2B was not
501 tasked during any active releases, meaning that future testing is needed to assess its detection
502 capabilities.

503
504 In practical applications for global remote sensing, teams have only limited information about
505 the location of possible sources and their likelihood of emitting at visible levels. As a result, it is
506 possible that the known-location experimental design applied here may have allowed teams to
507 artificially boost detection sensitivity to levels that would be difficult to achieve in general
508 practice.

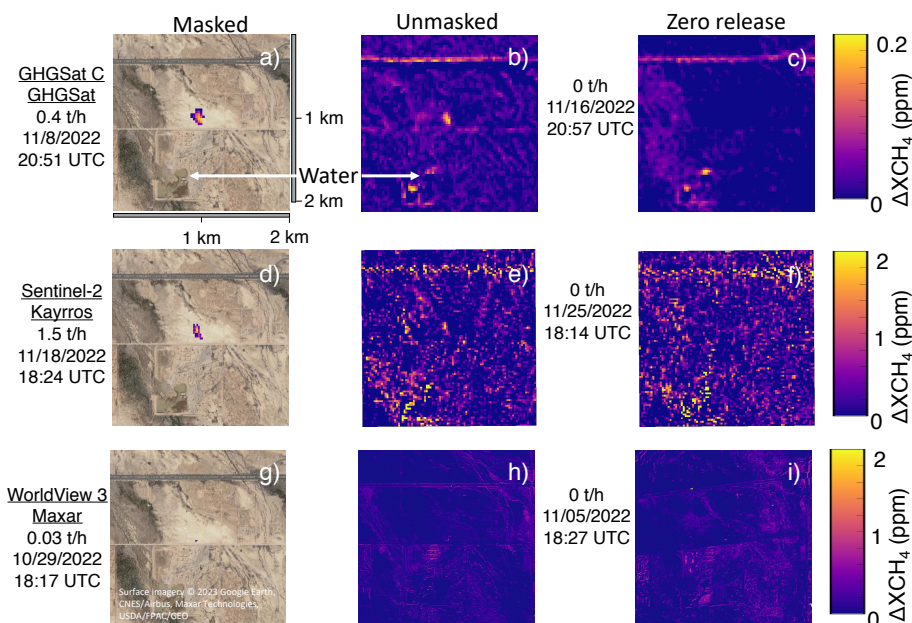
509
510 To qualitatively assess this possibility, all teams were required to submit methane retrieval field
511 images for all submitted estimates, including both detections and non-detections. In all cases,
512 teams submitted full-scene retrieval fields in a 2x2 km box around the release location. For
513 detected emissions, teams also submitted masked plume images, overlaying the estimated
514 methane plume above an optical image of the background location. See the SI, Section S4 for all
515 such images.

516
517 We highlight selected images in Figure 6 to showcase issues related to spectral artifacts, e.g.
518 apparent methane enhancements due to water bodies, clouds, or roads, that we were not able to
519 quantitatively address in this study. The GHGSat images, shown at a contrast-enhancing
520 narrower color scale of 0-0.2 ppm instead of this study's standard 2 ppm, show that for the
521 November 8th retrieval of the 0.401 [0.399, 0.404] t/h release, there are pixel clusters with
522 enhancements of comparable magnitude outside of the release area. However, these
523 enhancements are concentrated along ground features such as a water body southwest of the site
524 and a highway north of the site, confirmed in Google Maps imagery and WorldView-3 optical
525 images in the SI, Section S4. As a result, automated or manual intercomparison of the spatial
526 overlap of apparent methane enhancements and ground features visible in optical imagery could
527 plausibly help differentiate between such signal artifacts and true emissions. In some cases, it
528 may be possible to use measurements in which there is no evidence of a methane emission, e.g.
529 the November 16th measurement (in which GHGSat correctly determined the absence of methane
530 in a single-blind manner), to gain additional information into ambiguous cases. Artifacts such as

Deleted:

Deleted: The smallest detected emissions for the remaining satellites are 1.10 [1.06, 1.13] t/h for EnMAP, 1.26 [0.26, 2.26] t/h for GF5, 1.39 [1.34, 1.43] t/h for LandSat 8/9, 0.414 [0.410, 0.417] t/h for PRISMA, and 1.03 [0.98, 1.09] t/h for ZY1.

537 the water feature may consistently appear across retrievals, which could suggest that they are not
 538 true methane enhancements. Furthermore, GHGSat flagged the water body in both retrievals as a
 539 potential artifact, indicating that it would likely have been possible to correctly identify only the
 540 true methane emission in the November 8th scene even without a reference image with no
 541 methane.
 542



543 Figure 6. Masked and unmasked retrievals for selected emissions. In each case, the unmasked retrieval in the middle
 544 column appears to contain artifacts of similar intensity and shape to the masked emission. However, the emission
 545 may be more distinguishable from artifacts after intercomparison with ground features revealed through optical
 546 imagery, e.g. the water body southwest of the release site, and intercomparison with a reference day with zero
 547 emissions, as in the right column. Note that the GHGSat retrievals use a higher-contrast scale of 0-0.2 ppm. For See
 548 the SI, Section S4 for GHGSat images using the standard 0-2 ppm scale applied for most retrieval images in this
 549 study. Cloud-free surface imagery © 2023 Google Earth, CNES/Airbus, Maxar Technologies, USDA/FPAC/GEO.
 550

551 Sentinel-2 imagery is significantly noisier than most other tested satellites. The November 18th
 552 Kayrros retrieval in Figure 6 shows noticeable enhancements, comparable in intensity to the true
 553 emission, along the water feature and the highway, as well as northwest of the release site. In
 554 such a noise environment, knowledge of the emission location and access to images known not
 555 to contain emissions, such as panel f) may assist in correct identification of the true emission.
 556 See the SI, Section S4 for all masked and unmasked retrieval images from all satellites.
 557

558 Maxar correctly detected emissions as small as 0.0332 [0.0328, 0.0336] t/h using their
 559 WorldView-3 satellite on October 29th. Interestingly, their retrieval algorithm does not appear to
 560 introduce high-concentration artifacts over the water body (although that is not the case for all

561 teams analyzing WorldView-3 data, as shown in the SI, Section S4). The full retrieval image for
562 the October 29th retrieval shows concentration enhancement artifacts of comparable magnitude to
563 the correctly-detected emission at several points in the image. However, these artifacts are
564 largely conformal with surface features visible in optical imagery.

565
566 In addition to the known location, Maxar tasked its WorldView-3 satellite without notice to the
567 Stanford team on November 24th, a holiday in the United States. These data were shared with all
568 teams, but Maxar did not submit an unmasked image for the November 24th retrieval, although
569 they did for the zero-emission November 5th retrieval, shown in panel i). As a result, Maxar and
570 all other participating teams were able to compare satellite data from active testing days with
571 data that they knew very likely did not contain methane enhancements. As a result, these teams
572 had information in addition to the known release location that would not necessarily be available
573 in the field. As a result, we cannot definitively conclude from this study whether Maxar or other
574 teams would successfully identify emissions as small as 0.0332 [0.0328, 0.0336] t/h in the field.
575 Future testing, likely with multiple potential source locations, is needed to more rigorously
576 assess field-realistic detection limits of all satellites tested in this study.

577

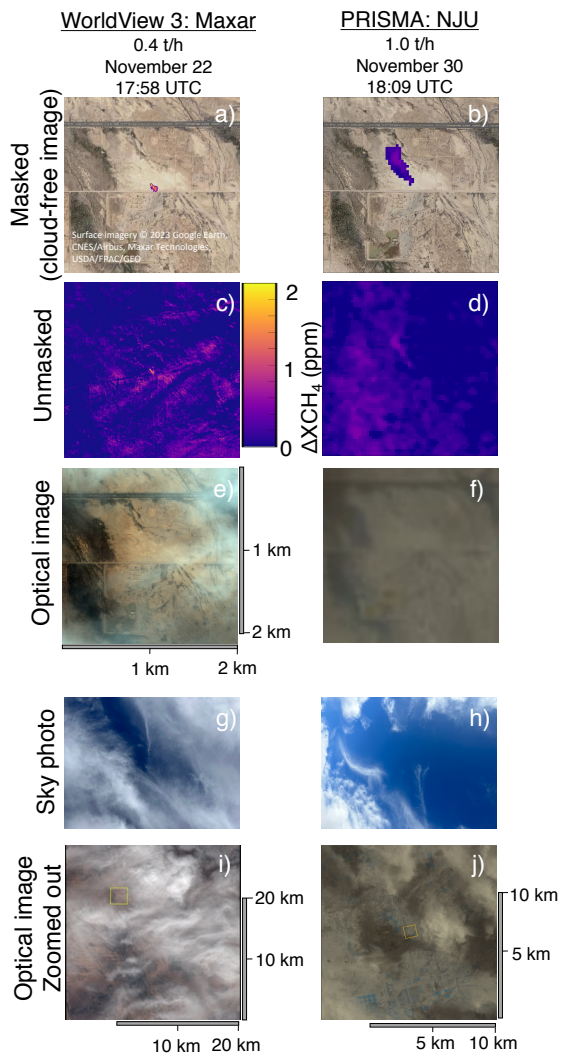
578 **2.4 The role of clouds**

579 Because water vapor is highly absorptive in the methane-active infrared frequencies targeted by
580 all nine methane-sensing satellites tested in this study, cloud cover can impede or prevent valid
581 satellite-based methane measurements. Although our Arizona test site was selected in part due to
582 its arid, relatively low-cloud climate, periodic cloud cover occurred to varying degrees
583 throughout the testing period.

584

585 The treatment of clouds varied across teams, with some filtering images due to cloud cover more
586 aggressively than others. LARS filtered the November 22nd WorldView-3 retrieval, shown in
587 Figure 7a, noting “the image is cloudy but we see some enhancement.” Kayrros and Maxar
588 correctly detected the 0.433 [0.430, 0.436] t/h emission for the same measurement, while NJU
589 reported a non-detection.

590



591
 592 Figure 7. Cloudy days with successful methane detections. a) and b) show masked methane emissions from
 593 WorldView-3 and PRISMA above a cloud-free standard background © 2023 Google Earth, CNES/Airbus, Maxar
 594 Technologies, USDA/FPAC/GEO. c) and d) show corresponding unmasked images. e) and f) show optical images
 595 of the same 2x2 km scene collected by each satellite. g) and h) show photographs of the sky, taken by Stanford
 596 researchers on smartphones at the time of each overpass. i) and j) show zoomed-out versions of the optical images
 597 shown in e) and f), with different length scales than the other panels.

598 This highlights that accurately interpreting the results of field measurements from each of these
599 teams requires an understanding of both detection performance and data filtering processes as a
600 function of cloud cover.

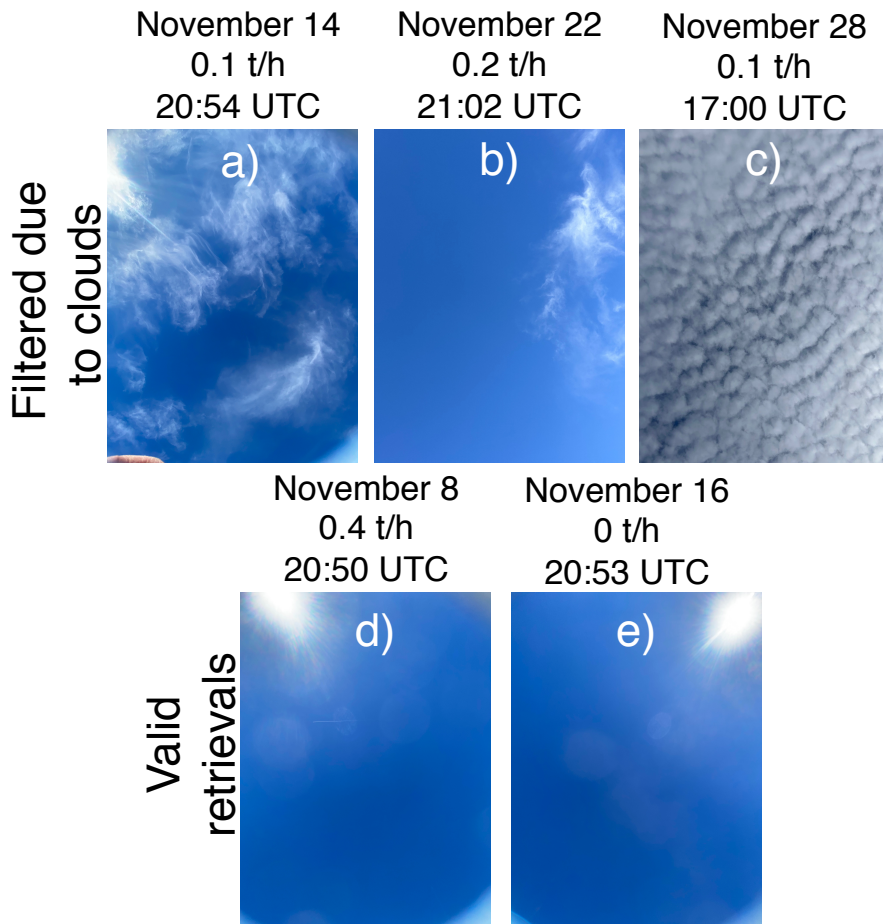
601
602 Stanford researchers took photographs of the sky coincident with most satellite overpasses to
603 document cloud cover, shown in full in the SI, Section S4. The photograph for the November
604 22nd WorldView-3 overpass, Figure 7g, appears to show significant thick cloud cover. However,
605 analysis of optical WorldView-3 imagery from this measurement, Figure 7e, shows that the area
606 immediately above the test site was relatively cloud-free even though the broader area was
607 experiencing significant cloud cover, shown in Figure 7i.

608
609 Analysis of the November 30th PRISMA measurement, shown in the second column of Figure 7
610 adds further nuance to the question of cloud cover. The sky photograph in Figure 7h shows the
611 presence of thin clouds. However, the optical image collected by PRISMA in Figure 7f shows no
612 clouds within the 2x2 km square surrounding the release site. The photographed clouds are only
613 visible in the larger, 14x14 km image in Figure 7j, which demonstrates that clouds are too far
614 away from the release site to interfere with the 0.98 [0.88, 1.08] t/h methane plume, which was
615 correctly detected by LARS, NJU, and Maxar.

616
617 These two cases demonstrate that only limited information regarding cloud cover can be
618 determined from single-frame sky photographs taken from the ground. This is particularly true
619 without clear orientation information, which is not available for the smartphone-based
620 photographs used in this study.

621
622 Figure 8 shows sky photographs of all dates with valid or operator-filtered GHGSat
623 measurements. Both days with valid measurements, one true positive and one true negative, were
624 essentially cloudless, as shown in Figure 8d-e. In addition, GHGSat filtered three retrievals due
625 to clouds. Of the three days filtered due to cloud cover, one was fully overcast (Figure 8c), while
626 two had thin clouds, shown in Figure 8a-b, also noted in the GHGSat report for those days. As
627 demonstrated above, it is difficult to determine from these sky photographs alone where these
628 clouds were in relation to the release site.
629

GHGSat-coincident sky photos



630 Figure 8. Ground-perspective sky photos for GHGSat-C measurements. a-c) correspond to measurements filtered
631 due to cloud cover. d) and e) correspond to valid retrievals, including one true positive detection and one true
632 negative non-detection. GHGSat-C satellites do not collect optical imagery, making it difficult to directly compare
633 ground-perspective photographs with satellite-perspective optical imagery.
634

635 GHGSat did not submit unmasked retrieval images for operator-filtered measurements (these
636 images were requested from all teams, but were not required as a condition of participation in
637 this test). Furthermore, GHGSat does not collect optical imagery in visible frequencies, so none

638 could be submitted. As a result, we can draw only limited conclusions about the role of cloud
639 cover in GHGSat's ability to conduct valid measurements with the GHGSat-C satellite model.

640
641 Future satellite-focused controlled methane release tests should further investigate the role of
642 cloud cover. This should include conducting testing in cloudier locations. In addition, sky
643 photographs should be replaced by or supplemented with passively-collected time series of
644 panoramic, georeferenced sky time series, e.g. using a fisheye camera, e.g., as used in solar
645 forecasting systems (Sun et al., 2018). This, together with optical images collected by satellites
646 (when available), will allow a more systematic evaluation of the capabilities of the tested
647 systems as a function of cloud cover. Such analysis should include assessment of the effect of
648 clouds on detection sensitivity and quantification performance, as well as their role in preventing
649 collection of valid measurements. These cloud-informed performance findings will be
650 indispensable in regional analysis of satellite-based methane remote sensing data, including its
651 incorporation into emissions inventories.

652

653 3 Discussion

654 This work demonstrates that all tested satellites are capable of detecting and quantifying methane
655 emissions. All eight satellites given the opportunity detected methane emissions, with overall
656 quantification accuracy similar, in percent terms, to aircraft-based methane sensing systems. This
657 highlights the large suite of satellite-based tools available to detect and quantify methane point
658 sources across the globe.

659
660 Detection limits appear to improve with smaller swath width and pixel size, and with higher
661 spectral resolution. Global-coverage satellites such as LandSat 8/9 and Sentinel-2, with swaths of
662 185 and 290 km, respectively, and spectral resolution 20-650 times coarser than the
663 hyperspectral instruments (EnMAP, PRISMA, GF5, ZY1, HJ2B, and GHGSat), have higher
664 detection limits. See the SI, Section S2 for additional discussion of spectral resolution. Our
665 results are consistent with (Gorroño et al., 2023), whose simulation-based approach suggests that
666 such instruments have a best-case minimum detection limit of roughly 1 t/h. Targeted satellites
667 with swaths of 30-60 km, including EnMAP, GF5, PRISMA, and ZY1 (EnMAP, 2023; Liu et al.,
668 2019; OHBI, 2022; Song et al., 2022), all reliably saw emissions of ~1 t/h. Of these, only
669 PRISMA has had the opportunity to be tested with emission fluxes below 1 t/h, correctly
670 detecting 0.413 [0.410, 0.417] t/h, the smallest emission given to PRISMA. GHGSat correctly
671 detected 0.401 [0.399, 0.403] t/h, with quantification accuracy within ±20%, using their
672 GHGSat-C-series satellite, with a swath width of 12 km. Estimates for smaller emission sizes
673 were filtered due to clouds, but in previous testing GHGSat successfully detected an 0.197
674 [0.187, 0.208] t/h emission and quantified it with similar accuracy, suggesting that the system
675 may be capable of seeing emissions even smaller than 200 kg/h.

676
677 Maxar successfully detected emissions as low as 0.0332 [0.0328, 0.0336] t/h using the
678 WorldView-3 satellite, with swath width 13.1 km. Two teams successfully detected emissions
679 below 0.1 t/h using WorldView-3, while two teams applied more conservative criteria and
680 detected only emissions above 0.5 t/h. Although Maxar has a coarser spectral resolution than
681 hyperspectral instruments, its very high spatial resolution enables heightened sensitivity.

682

Deleted: (

Deleted:)

Deleted: have

Deleted: Gorroño et al.

Deleted: Of these, only PRISMA was given smaller emissions, with three of four teams correctly detecting 0.413 [0.410, 0.417] t/h, the smallest emission given to PRISMA

690 In the high-emission New Mexico Permian basin oil and natural gas system, using 2019 emission
691 levels, a comprehensive measurement campaign with a constellation of satellites detecting all
692 emissions above 1 t/h would find 20% of emissions from oil and gas well sites, rising to 62% for
693 a satellite detecting emissions above 0.2 t/h, and 83% above 0.03 t/h (Sherwin et al., 2023b).

694 These fractions are upper-bound estimates both because near-real-time comprehensive coverage
695 would be challenging for satellite systems and because the underlying emission size distribution
696 estimate may be conservative for emissions below roughly 50 kg/hr (Sherwin et al., 2023b). In
697 lower-emitting basins such as the Denver-Julesburg, each of these systems would see a much
698 smaller fraction of total emissions, highlighting the need for a variety of technology approaches,
699 tailored to regional system characteristics (Sherwin et al., 2023b).

700
701 Note that the detection results presented in this paper reflect system performance with a known
702 source location under favorable desert climate conditions. These results may not translate to field
703 performance in different environments and with less foreknowledge about the location of
704 possible sources.

705
706 Unmasked methane retrieval fields, submitted by all teams, suggest that achievable detection
707 limits may be higher in practice for some satellites. In some cases, these images contain
708 background artifacts with estimated methane enhancements comparable in magnitude and
709 qualitatively similar in shape to the detected methane plumes. However, in many of these
710 retrieval fields, particularly for larger emissions, the true methane plume is unambiguous. It is
711 noteworthy that some teams correctly flagged likely background artifacts in blinded submissions,
712 but such georeferenced quality flagging was not required of all participating teams, although
713 doing so may be advisable in future tests.

714
715 The role of surface features, such as water bodies, in creating apparent methane enhancements
716 should be explored further. For example, the retrieval field for the 0.401 [0.399, 0.403] t/h
717 GHGSat measurement shows an apparent methane enhancement over a water body that is similar
718 in magnitude to the detected plume. However, if this is a known characteristic of the algorithm,
719 then such artifacts could be automatically or manually filtered out, leaving only the clear
720 methane plume at the release site. The water body appears as a flagged region in all data reported
721 by GHGSat, indicating that their system is capable of identifying potential confounding factors
722 such as water bodies and differentiating any resulting artifacts from true methane emissions.

723
724 Clouds add several levels of complexity to satellite-based methane sensing. The water vapor in
725 clouds interferes with the frequencies all tested satellites use to identify methane enhancements.
726 Heavy cloud cover essentially prevents valid satellite-based methane sensing. This test
727 demonstrates that it is possible in some circumstances to detect and quantify methane emissions
728 even in the presence of nearby patchy or thin clouds. However, it is unclear in some cases
729 whether these detected emissions would have been distinguishable from background noise, e.g.
730 artifacts caused by clouds or highly reflective/absorptive surface features, in the absence of a
731 known source location and reasonable anticipation of the presence of an emission due to an
732 ongoing test.

733
734 Different teams employed different filtering criteria. GHGSat excluded all GHGSat-C
735 measurements with cloud cover. Maxar and Kayrros used WorldView-3 to successfully detected

736 a 0.433 [0.430, 0.436] t/h emission on a cloudy day on November 22nd, while LARS filtered the
737 measurement due to clouds and NJU reported a non-detection.

Formatted: Superscript

738
739 Future testing should characterize the cloud conditions under which valid point-source methane
740 measurements can and cannot be conducted with each satellite-based system. In addition, future
741 work should characterize the effect of partial cloud cover on detection and quantification
742 performance. Understanding these two factors will be critical when interpreting the results of
743 large-scale satellite-based methane measurement campaigns, which will inevitably encounter
744 interference from clouds. Cloud cover varies widely across oil and gas-producing regions, with
745 limited clouds in arid areas such as the Permian basin in Texas and New Mexico, and significant
746 cloud cover in more temperate producing regions such as the Appalachian basin in the eastern
747 United States and the Williston basin in the midwestern United States (NASA, 2023).

748
749 It is noteworthy that even under cloud-free conditions, a targeted satellite overpass is not
750 guaranteed to produce valid data. Errors in tasking software, as well as onboard hardware upsets
751 can prevent valid data collection. The incidence of both in this paper may not be representative
752 of field performance for the tested technologies. Additional data collection, ideally from field
753 data, would be needed to accurately quantify the incidence of data collection failure, and further
754 location-specific analysis of cloud trends would be needed to understand the impact of cloud
755 cover on satellite data collection capabilities in a specific area.

756
757 Wind speed remains a major driver of uncertainty in satellite-based methane point source
758 quantification. Moving from wind reanalysis data to in situ wind measurements substantially
759 reduces scatter around the line of best fit, as was also the case in other work from the same group
760 (Sherwin et al., 2023b). In addition, in situ wind measurements show considerable temporal
761 variability in wind speed and direction over the multi-minute timescales most relevant to plume
762 formation.

763
764 In the field, winds are generally only available from reanalysis data, which capture temporal,
765 spatial, and directional variability with much lower fidelity than on-the-ground wind
766 measurements. Advances in the spatial and temporal fidelity of wind reanalysis products, as well
767 as their accuracy, could help improve methane remote sensing. In addition, it may be possible to
768 entirely eliminate reliance on wind speed, e.g. by inferring emission rate information solely from
769 plume shapes as in reference (Jongaramrungruang et al., 2022).

770
771 It is important to note that conducting this test did require the release of considerable amounts of
772 methane into the atmosphere. We estimate total emissions from the satellite testing discussed in
773 this paper at 7.7 t(CH₄), discussed further in the SI, Section S1.5. However, this pales in
774 comparison with anthropogenic emissions occurring across the globe. Lauvaux et al. identify
775 over 1000 emission sources across the world emitting at least 7.7 t(CH₄) every hour, in some
776 cases over 50 times as much every hour (Lauvaux et al., 2022). If this work assists in
777 accelerating mitigation of even one of these emissions by even a single hour, e.g. by ensuring
778 key decision-makers view satellite-based methane detection and quantification as reliable, we
779 will have broken even from a methane emissions perspective.

Formatted: Subscript

781

782 The findings presented here demonstrate that at least eight distinct satellite systems from three
783 continents are capable of detecting methane point sources of 1.5 t/h or less. Furthermore, this
784 study more systematically probes lower detection limits of these systems, two teams detecting
785 emissions below 0.1 t/h, the first time to our knowledge that such performance has been
786 demonstrated in a single-blind test of satellite-based methane sensing systems.

787
788 These satellites can play an important role in reducing methane emissions through existing
789 regulatory pathways, both in the United States and internationally. The US Environmental
790 Protection Agency’s proposed update to rules governing methane emissions from oil and natural
791 gas production includes a super-emitter response program, in which approved third-party data
792 providers can flag identified emissions above 0.1 t/h, obliging operators to investigate further
793 and, if necessary, take action to halt any further emissions (EPA, 2022). A proposed update to
794 the EPA Greenhouse Gas Reporting Program also includes a new category of “Other large
795 release” for inclusion in company emissions reports (EPA, 2023). The Methane Alert and
796 Response Systems, part of the United Nations’ International Methane Emissions Observatory,
797 uses vetted satellite data to notify governments, and in some cases operators, of large emissions
798 detected by satellite, with the aim of mitigating these emissions (IMEO, 2023). The eight
799 satellite systems tested with at least one nonzero emission in this study can provide high-quality
800 data to each of these programs.

801
802 In coming years, the Carbon Mapper and MethaneSAT systems will launch, alongside additional
803 satellites in some of the constellations tested here (Jacob et al., 2022). The airplane-mounted
804 precursors to both the Carbon Mapper and MethaneSAT systems have conducted substantial
805 single-blind testing of their point-source detection and quantification capabilities (Rutherford et
806 al., 2023; Chulakadabba et al., 2023; El Abbadi et al., 2023), but the satellites will require
807 additional tests. Furthermore, the NASA Earth Surface Mineral Dust Source Investigation
808 (EMIT) system, which launched shortly before our testing began (Wang and Lee, 2022), has
809 already reported detecting methane emissions in the field and should be tested, along with the
810 HJ2 system, in future single-blind controlled methane releases.

811
812 The tools exist for multi-lateral global methane monitoring efforts, with satellites from multiple
813 countries and continents able to independently assess emissions from regions of interest. The
814 single-blind test conducted here is a step toward ensuring that stakeholders across the world have
815 confidence in the methane emissions these satellite systems find at oil and gas facilities, landfills,
816 coal mines, and other emitting infrastructure. This will help satellites achieve their potential to
817 not only detect and quantify large methane emissions, but to inspire meaningful action to reduce
818 emissions of this powerful greenhouse gas.
819

820 4 Data and code availability

821 All data and code required to reproduce the figures and analysis in this paper are available at:
822 <https://github.com/sahar-elabbadi/SU-Controlled-Releases-2022>. Underlying spectral imagery
823 will not be made directly available through this study, but for many satellites tested in this study
824 these spectral data can be acquired either for free or for purchase for via platforms discussed in
825 the SI, Section S2.

Moved down [1]: The NASA Earth Surface Mineral Dust Source Investigation (EMIT), which launched shortly before our testing began³⁹, has already reported detecting methane emissions in the field and should be tested, along with the HJ2 system, in future single-blind controlled methane releases.

Deleted: ¶

Moved (insertion) [1]

Deleted: T

Deleted: will be made

Deleted: publicly

Deleted: on GitHub

837 **5 Abbreviations**

838

ADED	Advancing Development of Emissions Detection
ASI	Italian Space Agency
CNG	Compressed Natural Gas
EMIT	Earth Surface Mineral Dust Source Investigation
EnMAP	Environmental Mapping and Analysis Program
GF5	Gaofen 5
GSC	GHGSat-C (satellite)
HJ2	Huanjing 2
IME	Integrated Mass Enhancement
kg/h	Kilograms per hour
LARS	Land and Atmosphere Remote Sensing
LS	LandSat
METEC	Methane Emissions Technology Evaluation Center
NASA	National Aeronautics and Space Administration
NJU	Nanjing University
NOAA	National Oceanographic and Atmospheric Administration
OHB	Orbitale Hochtechnologie Bremen
PRISMA	PRecursores IperSpettrale della Missione Applicativa
UPV	Universitat Politècnica de València
USGS	United States Geological Survey
SRON	Stichting Ruimte Onderzoek Nederland
SWIR	Short-wave Infrared
TROPOMI	TROPospheric Monitoring Instrument
t/h	Metric tons per hour
VNIR	Visible to Near Infrared
WAV-P	Wide-Angle Fabry-Perot
WV3	WorldView-3
ZY1	Ziyuan 1

839

840 **6 Acknowledgments**

841 We acknowledge C. de Franchis, C. Giron, and A. Groshenry of Kayrros; and Z. Mouton, W.
 842 Kingwill, and R. Huppertz from Orbio Earth for their participation in this test. A. Esparza, L.
 843 Clark-Squire, J.F. Gauthier, M. Girard, D. Jervis, R. Mattson, J. McKeever, A. Newhook, and M.
 844 Turenne of GHGSat; J. Gorroño Viñepla, J. Roger Juan, and L. Guanter Palomar of LARS; Chen
 845 H., Li F., and Zhang H. of NJU; A. Hayden, J. Jonik, and J. Christy of Maxar both for
 846 participating in the test and for coordinating tasking and data sharing from key satellites. We
 847 acknowledge the German Aerospace Center and the Italian Space Agency for tasking the
 848 EnMAP and PRISMA satellites, respectively. Rawhide Leasing (Dana Walker) and Volta
 849 Fabrication (Mike Brandon, Walt Godsil, S.M., Merritt Norton) provided indispensable
 850 operational, logistical, and planning support for the experiment.

851 **7 Author contributions**

852 Conceptualization – EDS and ARB. Methods – EDS, SHE, YC, JSR, and ARB. Software – EDS,
853 PMB, ZC, and SHE. Validation – EDS. Formal analysis – EDS, PMB, ZZ, and SHE.
854 Investigation – EDS and SHE. Resources – ARB. Data curation – EDS, PMB, YC, ZZ, ZC, JSR,
855 and SHE. Writing: original draft – EDS. Writing: review and editing – All authors. Supervision –
856 EDS and ARB. Project administration – EDS, SEA, and ARB. Funding acquisition – EDS, SHE,
857 ARB. This work was supported by the US Department of Energy, Office of Science through
858 contract DE-AC02-05CH11231 between Lawrence Berkeley National Laboratory and the US
859 Department of Energy. The US government retains, and the publisher, by accepting the article
860 for publication, acknowledges that the US government retains, a non-exclusive, paid-up,
861 irrevocable, world-wide license to publish or reproduce the published form of this manuscript, or
862 allow others to do so, for US government purposes.

863 **8 Supplementary information available**

864 The online version contains supplementary material.

865 **9 Funding sources**

866 This study was funded by: The Environmental Defense Fund, the Global Methane Hub, the
867 International Methane Emissions Observatory, and the Stanford Natural Gas Initiative, an
868 industry consortium that supports independent research at Stanford University.

869 **10 Competing interests**

870 ARB serves on the Science and Measurement advisory committee of Carbon Mapper, which
871 plans to launch a methane-sensing satellite. YC and ZZ previously worked as interns at Carbon
872 Mapper. The remaining authors have no competing interests to declare.

873 **11 References**

- 874 Bell, C., Rutherford, J., Brandt, A., Sherwin, E., Vaughn, T., and Zimmerle, D.: Single-blind
875 determination of methane detection limits and quantification accuracy using aircraft-based
876 LiDAR, *Elementa: Science of the Anthropocene*, 10, 00080,
877 <https://doi.org/10.1525/elementa.2022.00080>, 2022.
- 878 Bell, C., Ilonze, C., Duggan, A., and Zimmerle, D.: Performance of Continuous Emission
879 Monitoring Solutions under a Single-Blind Controlled Testing Protocol, *Environ. Sci. Technol.*,
880 57, 5794–5805, <https://doi.org/10.1021/acs.est.2c09235>, 2023.
- 881 Bell, C. S., Vaughn, T. L., Zimmerle, D., Herndon, S. C., Yacovitch, T. I., Heath, G. A., Pétron,
882 G., Edie, R., Field, R. A., Murphy, S. M., Robertson, A. M., and Soltis, J.: Comparison of
883 methane emission estimates from multiple measurement techniques at natural gas production
884 pads, *Elementa: Science of the Anthropocene*, 5, 79, <https://doi.org/10.1525/elementa.266>, 2017.
- 885 Bell, C. S., Vaughn, T., and Zimmerle, D.: Evaluation of next generation emission measurement
886 technologies under repeatable test protocols, *Elementa: Science of the Anthropocene*, 8, 32,
887 <https://doi.org/10.1525/elementa.426>, 2020.

888 Chen, Y., Sherwin, E. D., Berman, E. S. F., Jones, B. B., Gordon, M. P., Wetherley, E. B., Kort,
889 E. A., and Brandt, A. R.: Quantifying Regional Methane Emissions in the New Mexico Permian
890 Basin with a Comprehensive Aerial Survey, *Environ. Sci. Technol.*, 56, 4317–4323,
891 <https://doi.org/10.1021/acs.est.1c06458>, 2022.

892 Chulakadabba, A., Sargent, M., Lauvaux, T., Benmergui, J. S., Franklin, E., Miller, C. C.,
893 Wilzewski, J. S., Roche, S., Conway, E., Souri, A. H., Sun, K., Luo, B., Hawthorne, J., Samra, J.,
894 Daube, B. C., Liu, X., Chance, K., Li, Y., Gautam, R., Omara, M., Rutherford, J. S., Sherwin, D.,
895 Brandt, A., and Wofsy, S. C.: Methane Point Source Quantification Using MethaneAIR: A New
896 Airborne Imaging Spectrometer, 2023.

897 Cusworth, D. H., Duren, R. M., Thorpe, A. K., Olson-Duvall, W., Heckler, J., Chapman, J. W.,
898 Eastwood, M. L., Helmlinger, M. C., Green, R. O., Asner, G. P., Dennison, P. E., and Miller, C.
899 E.: Intermittency of Large Methane Emitters in the Permian Basin, *Environ. Sci. Technol. Lett.*,
900 8, 567–573, <https://doi.org/10.1021/acs.estlett.1c00173>, 2021.

901 Cusworth, D. H., Thorpe, A. K., Ayasse, A. K., Stepp, D., Heckler, J., Asner, G. P., Miller, C. E.,
902 Yadav, V., Chapman, J. W., Eastwood, M. L., Green, R. O., Hmiel, B., Lyon, D. R., and Duren,
903 R. M.: Strong methane point sources contribute a disproportionate fraction of total emissions
904 across multiple basins in the United States, *Proc. Natl. Acad. Sci. U.S.A.*, 119, e2202338119,
905 <https://doi.org/10.1073/pnas.2202338119>, 2022.

906 Duren, R. M., Thorpe, A. K., Foster, K. T., Rafiq, T., Hopkins, F. M., Yadav, V., Buc, B. D.,
907 Thompson, D. R., Conley, S., Colombi, N. K., Frankenberg, C., McCubbin, I. B., Eastwood, M.
908 L., Falk, M., Herner, J. D., Croes, B. E., Green, R. O., and Miller, C. E.: California’s methane
909 super-emitters, *Nature*, 575, 180–184, <https://doi.org/10.1038/s41586-019-1720-3>, 2019.

910 El Abbadi, S., Chen, Z., Burdeau, P., Rutherford, J., Chen, Y., Zhang, Z., Sherwin, E., and
911 Brandt, A.: Comprehensive evaluation of aircraft-based methane sensing for greenhouse gas
912 mitigation, *Engineering*, <https://doi.org/10.31223/X51D4C>, 2023.

913 EnMAP: EnMAP: Mission, EnMAP, EnMAP, 2023.

914 EPA: Standards of Performance for New, Reconstructed, and Modified Sources and Emissions
915 Guidelines for Existing Sources: Oil and Natural Gas Sector Climate Review, 40 CFR Part 60,
916 87, 2022.

917 EPA: Greenhouse Gas Reporting Rule: Revisions and Confidentiality Determinations for
918 Petroleum and Natural Gas Systems, 40 CFR Part 98, 88, 2023.

919 ESA: eoPortal: PRISMA (Hyperspectral), European Space Agency, Paris, France, 2012.

920 ESA: Sentinel-2, European Space Agency, Paris, France, 2021a.

921 ESA: Sentinel-5P, European Space Agency, Paris, France, 2021b.

922 ESA: About GHGSat, European Space Agency, Paris, France, 2022a.

- 923 ESA: Earth Online: Worldview-3, European Space Agency, Paris, France, 2022b.
- 924 ESA: Sentinel Online: Sentinel-2, European Space Agency, Paris, France, 2022c.
- 925 GHGSat: Global leader in remote sensing of greenhouse gas, GHGSat, Montreal, Canada, 2022.
- 926 Gorroño, J., Varon, D. J., Irakulis-Loitxate, I., and Guanter, L.: Understanding the potential of
927 Sentinel-2 for monitoring methane point emissions, *Atmos. Meas. Tech.*, 16, 89–107,
928 <https://doi.org/10.5194/amt-16-89-2023>, 2023.
- 929 Guanter, L., Irakulis-Loitxate, I., Gorroño, J., Sánchez-García, E., Cusworth, D. H., Varon, D. J.,
930 Cogliati, S., and Colombo, R.: Mapping methane point emissions with the PRISMA spaceborne
931 imaging spectrometer, *Remote Sensing of Environment*, 265, 112671,
932 <https://doi.org/10.1016/j.rse.2021.112671>, 2021.
- 933 Hayden, A. and Christy, J.: Maxar’s WorldView-3 Enables Low-Concentration Methane
934 Detection from Space, <https://doi.org/10.31223/X51T1C>, 15 June 2023.
- 935 IMEO: Methane Alert and Response System (MARS), United Nations Environment Programme,
936 International Methane Emissions Observatory, Paris, France, 2023.
- 937 Irakulis-Loitxate, I., Guanter, L., Liu, Y.-N., Varon, D. J., Maasackers, J. D., Zhang, Y.,
938 Chulakadabba, A., Wofsy, S. C., Thorpe, A. K., Duren, R. M., Frankenberg, C., Lyon, D. R.,
939 Hmiel, B., Cusworth, D. H., Zhang, Y., Segl, K., Gorroño, J., Sánchez-García, E., Sulprizio, M.
940 P., Cao, K., Zhu, H., Liang, J., Li, X., Aben, I., and Jacob, D. J.: Satellite-based survey of
941 extreme methane emissions in the Permian basin, *Sci. Adv.*, 7, eabf4507,
942 <https://doi.org/10.1126/sciadv.abf4507>, 2021.
- 943 Irakulis-Loitxate, I., Gorroño, J., Zavala-Araiza, D., and Guanter, L.: Satellites Detect a Methane
944 Ultra-emission Event from an Offshore Platform in the Gulf of Mexico, *Environ. Sci. Technol.*
945 *Let.*, 9, 520–525, <https://doi.org/10.1021/acs.estlett.2c00225>, 2022a.
- 946 Irakulis-Loitxate, I., Guanter, L., Maasackers, J. D., Zavala-Araiza, D., and Aben, I.: Satellites
947 Detect Abatable Super-Emissions in One of the World’s Largest Methane Hotspot Regions,
948 *Environ. Sci. Technol.*, 56, 2143–2152, <https://doi.org/10.1021/acs.est.1c04873>, 2022b.
- 949 Jacob, D. J., Varon, D. J., Cusworth, D. H., Dennison, P. E., Frankenberg, C., Gautam, R.,
950 Guanter, L., Kelley, J., McKeever, J., Ott, L. E., Poulter, B., Qu, Z., Thorpe, A. K., Worden, J.
951 R., and Duren, R. M.: Quantifying methane emissions from the global scale down to point
952 sources using satellite observations of atmospheric methane, *Atmos. Chem. Phys.*, 22, 9617–
953 9646, <https://doi.org/10.5194/acp-22-9617-2022>, 2022.
- 954 Jervis, D., McKeever, J., Durak, B. O. A., Sloan, J. J., Gains, D., Varon, D. J., Ramier, A.,
955 Strupler, M., and Tarrant, E.: The GHGSat-D imaging spectrometer, *Atmos. Meas. Tech.*, 14,
956 2127–2140, <https://doi.org/10.5194/amt-14-2127-2021>, 2021.
- 957 Jia, M., Li, F., Zhang, Y., Wu, M., Li, Y., Feng, S., Wang, H., Chen, H., Ju, W., Lin, J., Cai, J.,
958 Zhang, Y., and Jiang, F.: The Nord Stream pipeline gas leaks released approximately 220,000

959 tonnes of methane into the atmosphere, *Environmental Science and Ecotechnology*, 12, 100210,
960 <https://doi.org/10.1016/j.ese.2022.100210>, 2022.

961 Jongaramrungruang, S., Thorpe, A. K., Matheou, G., and Frankenberg, C.: MethaNet – An AI-
962 driven approach to quantifying methane point-source emission from high-resolution 2-D plume
963 imagery, *Remote Sensing of Environment*, 269, 112809,
964 <https://doi.org/10.1016/j.rse.2021.112809>, 2022.

965 Kayrros: A partner for today and the future, agile with technology and with a smarter approach
966 to data, Kayrros, Paris, France, 2022.

967 Lauvaux, T., Giron, C., Mazzolini, M., d'Aspremont, A., Duren, R., Cusworth, D., Shindell, D.,
968 and Ciais, P.: Global Assessment of Oil and Gas Methane Ultra-Emitters, *Science*, 375, 557–
969 561, <https://doi.org/10.31223/X5NS54>, 2022.

970 Liu, Y.-N., Zhang, J., Zhang, Y., Sun, W.-W., Jiao, L.-L., Sun, D.-X., Hu, X.-N., Ye, X., Li, Y.-
971 D., Liu, S.-F., Cao, K.-Q., Chai, M.-Y., and Zhou, W.-Y.-N.: The Advanced Hyperspectral
972 Imager: Aboard China's GaoFen-5 Satellite, *IEEE Geosci. Remote Sens. Mag.*, 7, 23–32,
973 <https://doi.org/10.1109/MGRS.2019.2927687>, 2019.

974 Luo, H., Li, Z., Wu, Y., Qiu, Z., Shi, H., Wang, Q., and Xiong, W.: Greenhouse Gases
975 Monitoring Instrument on GaoFen-5 Satellite-II: Optical Design and Evaluation, *Remote
976 Sensing*, 15, 1105, <https://doi.org/10.3390/rs15041105>, 2023.

977 NASA: NASA Earth Observations Cloud Fraction (1 Month TERRA/MODIS), National
978 Aeronautics and Space Administration, Washington, D.C., 2023.

979 OHBI: Satellites & Missions: PRISMA, Orbitale Hochtechnologie Bremen Italia S.p.A., Milan,
980 Italy, 2022.

981 Orbio: Actionable Methane Intelligence: Filling the global methane gap with asset-level
982 emissions data, Orbio, Köln, Germany, 2023.

983 Pandey, S., Gautam, R., Houweling, S., van der Gon, H. D., Sadavarte, P., Borsdorff, T.,
984 Hasekamp, O., Landgraf, J., Tol, P., van Kempen, T., Hoogeveen, R., van Hees, R., Hamburg, S.
985 P., Maasackers, J. D., and Aben, I.: Satellite observations reveal extreme methane leakage from a
986 natural gas well blowout, *Proc. Natl. Acad. Sci. U.S.A.*, 116, 26376–26381,
987 <https://doi.org/10.1073/pnas.1908712116>, 2019.

988 Ravikumar, A. P., Sreedhara, S., Wang, J., Englander, J., Roda-Stuart, D., Bell, C., Zimmerle,
989 D., Lyon, D., Mogstad, I., Ratner, B., and Brandt, A. R.: Single-blind Inter-comparison of
990 Methane Detection Technologies - Results from the Stanford/EDF Mobile Monitoring
991 Challenge, *Elementa: Science of the Anthropocene*, 7, 29, <https://doi.org/10.1525/elementa.373>,
992 2019.

993 Roger, J., Irakulis-Loitxate, I., Valverde, A., Gorroño, J., Chabrilat, S., Brell, M., and Guanter,
994 L.: High-resolution methane mapping with the EnMAP satellite imaging spectroscopy mission,
995 *Atmospheric Sciences*, <https://doi.org/10.31223/X5M65Z>, 2023.

996 Rutherford, J., Sherwin, E., Chen, Y., Aminfard, S., and Brandt, A.: Evaluating methane
997 emission quantification performance and uncertainty of aerial technologies via high-volume
998 single-blind controlled releases, *Oil, Gas, and Energy*, <https://doi.org/10.31223/X5KQ0X>, 2023.

999 Sánchez-García, E., Gorroño, J., Irakulis-Loitxate, I., Varon, D. J., and Guanter, L.: Mapping
1000 methane plumes at very high spatial resolution with the WorldView-3 satellite, *Environmental
1001 Science & Technology*, 56, 10517–10529, <https://doi.org/10.1021/acs.est.1c08575>, 2022.

1002 Scott, W.: Mapping Methane Emissions Using Maxar’s WorldView-3 Satellite, Maxar, Ann
1003 Arbor, MI, USA, 2022.

1004 Sherwin, E., Rutherford, J., Zhang, Z., Chen, Y., Wetherley, E., Yakovlev, P., Berman, E., Jones,
1005 B., Thorpe, A., Ayasse, A., Duren, R., Brandt, A., and Cusworth, D.: Quantifying oil and natural
1006 gas system emissions using one million aerial site measurements, In Review,
1007 <https://doi.org/10.21203/rs.3.rs-2406848/v1>, 2023a.

1008 Sherwin, E. D., Chen, Y., Ravikumar, A. P., and Brandt, A. R.: Single-blind test of airplane-
1009 based hyperspectral methane detection via controlled releases, *Elementa: Science of the
1010 Anthropocene*, 9, 00063, <https://doi.org/10.1525/elementa.2021.00063>, 2021.

1011 Sherwin, E. D., Rutherford, J. S., Chen, Y., Aminfard, S., Kort, E. A., Jackson, R. B., and
1012 Brandt, A. R.: Single-blind validation of space-based point-source detection and quantification of
1013 onshore methane emissions, *Sci Rep*, 13, 3836, <https://doi.org/10.1038/s41598-023-30761-2>,
1014 2023b.

1015 Song, Q., Ma, C., Liu, J., and Wei, H.: Quantifying ocean surface green tides using high-spatial
1016 resolution thermal images, *Opt. Express*, 30, 36592, <https://doi.org/10.1364/OE.472479>, 2022.

1017 Sun, Y., Szücs, G., and Brandt, A. R.: Solar PV output prediction from video streams using
1018 convolutional neural networks, *Energy Environ. Sci.*, 8, 2018.

1019 USGS: Landsat 8, United States Geological Survey, Washington, D.C., 2022.

1020 Varon, D. J., Jacob, D. J., McKeever, J., Jervis, D., Durak, B. O. A., Xia, Y., and Huang, Y.:
1021 Quantifying methane point sources from fine-scale satellite observations of atmospheric methane
1022 plumes, *Atmos. Meas. Tech.*, 11, 5673–5686, <https://doi.org/10.5194/amt-11-5673-2018>, 2018.

1023 Varon, D. J., McKeever, J., Jervis, D., Maasackers, J. D., Pandey, S., Houweling, S., Aben, I.,
1024 Scarpelli, T., and Jacob, D. J.: Satellite Discovery of Anomalously Large Methane Point Sources
1025 From Oil/Gas Production, *Geophys. Res. Lett.*, 46, 13507–13516,
1026 <https://doi.org/10.1029/2019GL083798>, 2019.

1027 Varon, D. J., Jervis, D., McKeever, J., Spence, I., Gains, D., and Jacob, D. J.: High-frequency
1028 monitoring of anomalous methane point sources with multispectral Sentinel-2 satellite
1029 observations, *Atmos. Meas. Tech.*, 14, 2771–2785, <https://doi.org/10.5194/amt-14-2771-2021>,
1030 2021.

- 1031 Wang, A. and Lee, J. J.: Methane ‘Super-Emitters’ Mapped by NASA’s New Earth Space
1032 Mission, National Aeronotics and Space Administration, Pasadena, California, USA, 2022.
- 1033 Xinhua: China launches new remote sensing satellite, XinhuaNet, 9th December, 2022.
- 1034 Zhang, B., Guo, B., Zou, B., Wei, W., Lei, Y., and Li, T.: Retrieving soil heavy metals
1035 concentrations based on GaoFen-5 hyperspectral satellite image at an opencast coal mine, Inner
1036 Mongolia, China, Environmental Pollution, 300, 118981,
1037 <https://doi.org/10.1016/j.envpol.2022.118981>, 2022.
- 1038 Zhong, B., Yang, A., Liu, Q., Wu, S., Shan, X., Mu, X., Hu, L., and Wu, J.: Analysis Ready Data
1039 of the Chinese GaoFen Satellite Data, Remote Sensing, 13, 1709,
1040 <https://doi.org/10.3390/rs13091709>, 2021.
- 1041 Zimmerle, D.: METEC Controlled Test Protocol: Survey Emission Detection And
1042 Quantification, Colorado State University, Fort Collins, CO, USA, 2022.
- 1043

Deleted: Supplementary information for “Single-blind test of nine methane-sensing satellite systems from three continents”[¶]

Authors: Evan D. Sherwin^{1,*}, Sahar H. El Abbadi¹, Philippine M. Burdeau¹, Zhan Zhang¹, Zhenlin Chen¹, Jeffrey S. Rutherford^{1,a}, Yuanlei Chen¹, Adam R. Brandt¹[¶]

Author Affiliations:[¶]

¹ Department of Energy Science & Engineering, Stanford University, Stanford, California 94305, United States [¶]

^a Present affiliation: Highwood Emissions Management, Calgary, Alberta T2P 2V1, Canada[¶]

* Correspondence: evands@stanford.edu[¶]

Table of contents[¶]

S1. Participating satellites [¶]

S2. Participating teams [¶]

S3. Supplementary methods[¶]

S4. Supplementary results[¶]

-----Page Break-----

Supplementary methods[¶]

Advancing Development of Emissions Detection Protocol[¶]

The single-blind controlled methane release testing in this study followed the Advancing Development of Emissions Detection (ADED) protocol, developed at the Methane Emissions Technology Evaluation Center (METEC) in Colorado (Zimmerle, 2022).[¶]

We followed protocols from Section 10, “Aerial Survey Emission Detection And Quantification,” which was designed to apply to remote sensing technologies in general, including satellites (Zimmerle, 2022).[¶]

Documentation of the system under test is included both within this paper as well as in the “Performer Info” tab of the data spreadsheets submitted by each team, which are available in the GitHub repository associated with this paper. Submitted emissions estimates used the standard template spreadsheet for the Aerial Survey Emission Detection And Quantification version of the ADED protocol (Zimmerle, 2022).[¶]

Following Section 10.1.1 of the ADED protocol, all teams were required to notify the Stanford team in advance of the flight patterns they intended to fly, including orientation. Teams were required to explain any deviations from this flight plan, e.g. due to inclement weather conditions (Zimmerle, 2022).[¶]

Following Section 10.4.1 of the ADED protocol, the test location was at least 1 km away from all potential confounding methane sources, e.g. the local landfill, and from all nearby water features (Zimmerle, 2022).[¶]

Flow rate estimation[¶]

Unless otherwise specified, all methane flow rate estimates are the average flow rate over the five minutes preceding a timestamp. Meters produce a whole-gas mass flow rate, which we convert to a methane flow rate using the methane fraction provided in natural gas composition measuremen... [4]

Page 5: [1] Deleted Evan Sherwin 9/29/23 11:01:00 AM

Page 5: [1] Deleted Evan Sherwin 9/29/23 11:01:00 AM

Page 5: [2] Formatted Evan Sherwin 10/18/23 2:30:00 PM

Font: 11 pt

Page 5: [2] Formatted Evan Sherwin 10/18/23 2:30:00 PM

Font: 11 pt

Page 5: [3] Deleted Evan Sherwin 9/29/23 11:03:00 AM

Page 5: [3] Deleted Evan Sherwin 9/29/23 11:03:00 AM

Page 5: [3] Deleted Evan Sherwin 9/29/23 11:03:00 AM

Page 1: [4] Deleted Evan Sherwin 10/20/23 7:18:00 PM